U.S. DEPARTMENT OF COMMERCE
NATIONAL OCEANIC AND ATMOSPHERIC ADMINISTRATION
NATIONAL WEATHER SERVICE
NATIONAL METEOROLOGICAL CENTER

OFFICE NOTE 395

DYNAMIC COUPLING BETWEEN THE NMC GLOBAL ATMOSPHERE AND SPECTRAL WAVE MODELS

D. Chalikov, D. Esteva, M. Iredell,
and P. Long

August 1993

U.S. DEPARTMENT OF COMMERCE
NATIONAL OCEANIC AND ATMOSPHERIC ADMINISTRATION
NATIONAL WEATHER SERVICE

TECHNICAL NOTE*

DYNAMIC COUPLING BETWEEN THE NMC GLOBAL ATMOSPHERE AND SPECTRAL WAVE MODELS

DMITRY CHALIKOV, DINORAH ESTEVA, MARK IREDELL,
AND PAUL LONG

AUGUST 1993

---

*OPC CONTRIBUTION NO. 78
NMC OFFICE NOTE NO. 395

OPC CONTRIBUTIONS

No. 1. Burroughs, L. D., 1986: Development of Forecast Guidance for Santa Ana Conditions. National Weather Digest, Vol. 12 No. 1, 8pp.

No. 2. Richardson, W. S., D. J. Schwab, Y. Y. Chao, and D. M. Wright, 1986: Lake Erie Wave Height Forecasts Generated by Empirical and Dynamical Methods -- Comparison and Verification. Technical Note, 23pp.

No. 3. Auer, S. J., 1986: Determination of Errors in LFM Forecasts Surface Lows Over the Northwest Atlantic Ocean. Technical Note/NMC Office Note No. 313, 17pp.

No. 4. Rao, D. B., S. D. Steenrod, and B. V. Sanchez, 1987: A Method of Calculating the Total Flow from A Given Sea Surface Topography. NASA Technical Memorandum 87799., 19pp.

No. 5. Feit, D. M., 1986: Compendium of Marine Meteorological and Oceanographic Products of the Ocean Products Center. NOAA Technical Memorandum NWS NMC 68, 93pp.

No. 6. Auer, S. J., 1986: A Comparison of the LFM, Spectral, and ECMWF Numerical Model Forecasts of Deepening Oceanic Cyclones During One Cool Season. Technical Note/NMC Office Note No. 312, 20pp.

No. 7. Burroughs, L. D., 1987: Development of Open Fog Forecasting Regions. Technical Note/NMC Office Note, No. 323., 36pp.

No. 8. Yu, T. W., 1987: A Technique of Deducing Wind Direction from Satellite Measurements of Wind Speed. Monthly Weather Review, 115, 1929-1939.

No. 9. Auer, S. J., 1987: Five-Year Climatological Survey of the Gulf Stream System and Its Associated Rings. Journal of Geophysical Research, 92, 11,709-11,726.

No. 10. Chao, Y. Y., 1987: Forecasting Wave Conditions Affected by Currents and Bottom Topography. Technical Note, 11pp.

No. 11. Esteva, D. C., 1987: The Editing and Averaging of Altimeter Wave and Wind Data. Technical Note, 4pp.

No. 12. Feit, D. M., 1987: Forecasting Superstructure Icing for Alaskan Waters. National Weather Digest, 12, 5-10.

No. 13. Sanchez, B. V., D. B. Rao, S. D. Steenrod, 1987: Tidal Estimation in the Atlantic and Indian Oceans. Marine Geodesy, 10, 309-350.

No. 14. Gemmill, W.H., T.W. Yu, and D.M. Feit 1988: Performance of Techniques Used to Derive Ocean Surface Winds. Technical Note/NMC Office Note No. 330, 34pp.

No. 15. Gemmill, W.H., T.W. Yu, and D.M. Feit 1987: Performance Statistics of Techniques Used to Determine Ocean Surface Winds. Conference Preprint, Workshop Proceedings AES/CMOS 2nd Workshop of Operational Meteorology, Halifax, Nova Scotia., 234-243.

No. 16. Yu, T.W., 1988: A Method for Determining Equivalent Depths of the Atmospheric Boundary Layer Over the Oceans. Journal of Geophysical Research, 93, 3655-3661.

No. 17. Yu, T.W., 1987: Analysis of the Atmospheric Mixed Layer Heights Over the Oceans. Conference Preprint, Workshop Proceedings AES/CMOS 2nd Workshop of Operational Meteorology, Halifax, Nova Scotia, 2, 425-432.

No. 18. Feit, D. M., 1987: An Operational Forecast System for Superstructure Icing. Proceedings Fourth Conference Meteorology and Oceanography of the Coastal Zone. 4pp.

DYNAMIC COUPLING BETWEEN THE NMC GLOBAL ATMOSPHERE AND SPECTRAL WAVE MODELS

D. Chalikov, D. Esteva, M. Iredell, and P.Long

National Meteorological Center, Washington, D. C.

ABSTRACT

The theory and parameterization methods of small-scale ocean-atmosphere dynamical interaction are discussed. Two different theoretical approaches to the problem are briefly presented. One approach follows the one-dimensional theory proposed by Chalikov and Belevich and the other is Janssen's extension of the Miles' instability theory. Both approaches provide for coupling the lower portion of the marine boundary layer, the wave boundary layer, with the underlying wavy sea surface. The results of applying simplifications of each approach to couple the National Meteorological Center global atmosphere and spectral wave models are illustrated and compared. The effects, although small, are noticeable especially in areas of high winds.

1. INTRODUCTION

The local thermodynamic interaction between the ocean and the atmosphere is one of the primary mechanisms affecting the ocean-atmosphere system. Thus, the accuracy of the parameterization of this interaction determines to a considerable extent the quality of weather forecasts and climate modeling. Existing approaches to parameterize this microscale interaction do not take into account several mechanisms which influence both media. In this paper only the dynamical interaction is discussed, that is, the momentum exchange. However, the approach presented may be extended to take into account the sensible and latent heat exchanges and the effects of stratification.

A major concern in the theory of the planetary boundary layer is the establishment of an appropriate relation between the turbulent stress $\mathbf{T}$ (bold letters denote vector quantities), and the horizontal wind velocity vector, $\mathbf{u} = (u,v)$ at an arbitrary height, z. It is generally accepted that this relation takes the form

$$\boldsymbol{T} = \rho_a C_z \mid \boldsymbol{u} \mid \boldsymbol{u} , \qquad (1.1)$$

where ρ_a is the air density, and C_z is the drag coefficient at height z.

The value of C_z over land for neutral stratification depends upon the morphological surface characteristics, usually specified by the roughness parameter or roughness height z_o, which is related to C_z by

$$C_z = [\, K/(\ln(z/z_o))\,]^2 \,, \qquad (1.2)$$

where K is von Karman's constant.

The roughness height over the ocean is more complex due to the dynamics of the sea surface. It is customary to estimate z_o for a wavy sea surface with the formula suggested by Charnock (1955):

$$z_o = m\, u_*^2 \,/g \,, \qquad (1.3)$$

where g is the acceleration og gravity, u_* the friction velocity, and m is an empirical coefficient whose experimental value has been found to vary from 0.01 to 0.05 (Garratt, 1977). Even though expression (1.3) has been shown to provide a representative scale for the roughness height over the ocean, the large scatter of the empirical data indicates that it should be considered only as a qualitative relationship. The large scatter is in part explained by inaccuracies in the experimental technique, nonstationarity and inhomogeneity of the flow, and density stratification. Scatter may also be due to systematic deviations of the wind profile from logarithmic which are caused by wave-produced momentum fluxes. Finally, (1.3) appears to be valid only for a fully-developed sea in the absence of swell.

That the roughness length over the ocean depends on sea state (wave age) was suggested by Stewart (1967), Kitaigorodski (1968), Janssen (1982), and Donelan (1982). The nondimensional wave age μ is defined as $\mu = c_p/u_*$, where c_p is the phase speed of the dominant wind wave.

The variability of the wave field introduces inhomogeneities in the surface stress over the ocean which amplifies the vertical motions at the upper levels of the marine boundary layer. Thus, the sea state may very well affect weather evolution and climate.

The coupling between the wind and the waves was also considered by Jeffreys (1925), Miles (1957, 1960), Phillips (1957), Fabrikant (1976), Chalikov (1976, 1978, 1986), Janssen (1982, 1989), and Janssen et al. (1989). Janssen extended Miles' shear-flow mechanism by numerical solution of the Orr-Sommerfeld-Rayleigh (OSR) equation in tandem with a diffusion-like equation with a diffusion coefficient dependent on the wave spectrum and solutions to the OSR equation (Orr, 1907; Sommerfeld, 1980; Rayleigh, 1880). Expressing Phillips' constant as a power law with strong dependence on wave age which fits observed field wave spectra Janssen et al. (1984) found a strong coupling between the wind and waves for young (i.e. small wave age) wind waves, and a much weaker coupling for older waves. Janssen's approach was applied by Weber et al. (1992) to couple the wave model WAM (WAMDIG, 1988), to a general

atmospheric circulation model (ECHAM2, Roeckner et al., 1989). In the present study, a simplified form of the Janssen analysis is used which approximates the decrease in roughness length with wave age as found by Janssen.

Chalikov (1992) argued that Janssen's approach has some difficiencies that precludes its confident use to model the air-sea momentum transfer. In particular, Janssen's reduction of the air-sea momentum transfer to a diffusion-like equation amounts to a diffusion equation with an advection term proportional to the vertical derivative of the diffusion coefficient. It is unlikely that the momentum transfer may be modeled by such an advection/diffusion process (Chalikov, 1992).

2. WAVE BOUNDARY LAYER MODEL: CHALIKOV'S APPROACH

A summary of the wave boundary layer model proposed by Chalikov and Belevich (1992) is presented in this section. Consider the bottom portion of the marine atmospheric boundary layer, the wave boundary layer (WBL), to be a nonstationary layer with a structure approximately governed by the equation:

$$\frac{\partial \boldsymbol{u}}{\partial t} = \frac{\partial}{\partial z}(\boldsymbol{T} + \tau), \tag{2.1}$$

where z is a vertical coordinate which at small heights will be considered as a surface-following coordinate, (Chalikov and Belevich, 1992); $\mathbf{u}$ is the velocity vector; $\mathbf{T}$ and τ are respectively, the vertical fluxes of momentum due to turbulence and to wave-induced perturbations. $\mathbf{T}$ may be parameterized as

$$\boldsymbol{T} = K_M \frac{\partial \boldsymbol{u}}{\partial z}, \tag{2.2}$$

where K_M is the coefficient of turbulent viscosity. At a non-dimensional height $\xi = z/\lambda_a$, the wave induced momentum flux may be expressed as

$$\tau = \rho_w g \int_0^{\omega_r} \int_{-\pi}^{\pi} \boldsymbol{k} S(\omega, \theta)\, \beta(\varpi_a, C_\lambda)\, F(\varpi_a, C_\lambda, \xi)\, d\theta d\omega. \tag{2.3}$$

where ρ_w is the water density, g is the acceleration of gravity, and k is the wavenumber. The function $F(\hat{\omega}_a, C_\lambda, \xi)$ describes the vertical variation of wave-induced momentum flux for each nondimensional spectral frequency $\hat{\omega}_a$,

$$\varpi_a = \omega \mid \boldsymbol{u}_\lambda \mid \frac{\cos\theta}{g} \tag{2.4}$$

where $\mathbf{u}_\lambda$ is the wind velocity at a height $z = \lambda_a$:

$$\lambda_a = \frac{2\pi g}{\omega^2 \mid \cos\theta \mid} \tag{2.5}$$

is an apparent wavelength, and C_λ is the drag coefficient at height λ_a. The upper limit of integration ω_r is the highest frequency for which the wave spectrum S is known.

The function β is the nondimensional wind-wave growth parameter that is a function of $\breve{\omega}_a$ and C_λ. Approximations for F and β are given in Chalikov and Belevich (1992). These approximations were obtained from extensive numerical experiments using a 2-D model of the statistical structure of the WBL (Chalikov, 1978; 1986; Chalikov and Makin, 1991; Burgers and Makin, 1992). The wave growth parameter is defined as

$$\beta(\omega) = \frac{\rho_a}{\rho_w} \frac{\mathscr{E}(\omega)}{\omega\, S(\omega)} \tag{2.6}$$

where $\mathscr{E}(\omega)$ is the energy flux from the wind to the waves divided by the air density. β may be approximated as

$$10^4\beta = \begin{pmatrix} -a_1\varpi_a^2 - a_2 & , \ \varpi_a \le -1 \\ a_3\varpi_a\,(a_4\,\varpi_a - a_5) - a_6 & , \ \varpi_a \in \left(-1, \frac{\Omega_1}{2}\right) \\ (a_4\,\varpi_a - a_5)\,\varpi_a & , \ \varpi_a \in \left(\frac{\Omega_1}{2}, \Omega_1\right) \\ a_7\,\varpi_a - a_8 & , \ \varpi_a \in (\Omega_1, \Omega_2) \\ a_9\,(\varpi_a - 1)^2 + a_{10} & , \ \varpi_a > \Omega_2 \end{pmatrix}. \tag{2.7}$$

In (2.7) a_1 through a_{10} and Ω_1 and Ω_2, are parameters depending on C_λ and are given by

$$\begin{aligned} \Omega_1 &= 1.075 + 75C_\lambda, & \Omega_2 &= 1.2 + 300C_\lambda \\ a_1 &= 0.25 + 395C_\lambda, & a_3 &= (a_o - a_2 - a_1)/(a_o + a_4 + a_5) \\ a_2 &= 0.35 + 150C_\lambda, & a_5 &= a_4\,\Omega_1 \\ a_4 &= 0.30 + 300C_\lambda, & a_6 &= a_o\,(1 - a_9) \\ a_9 &= 0.35 + 240C_\lambda, & a_7 &= (a_9(\Omega_2 - 1)^2 + a_{10})/(\Omega_2 - \Omega_1) \\ a_{10} &= -0.06 + 470C_\lambda, & a_8 &= a_7\Omega_1 \\ a_o &= 0.25\, a_5^2/a_4. \end{aligned} \tag{2.8}$$

For frequencies $|\breve{\omega}_a| \geq 2$ the parameter β depends on $\breve{\omega}_a^2$ and, therefore, on the square of the wind speed. This dependence is confirmed by the experimental data of Hsiao and Shemdin (1983), and is more representative than the linear dependence derived from the field data of Snyder et al. (1981). High frequency waves are nearly stationary relative to the wind; thus, their drag in turbulent flow is likely to have a quadratic dependence on wind speed, as is the case for stationary roughness elements. The linear dependence of β on $\breve{\omega}_a$ exists only for $\breve{\omega}_a \in (\Omega_1, \Omega_2)$. For $\breve{\omega}_a \leq -1$, β becomes negative. This case corresponds to waves traveling against the wind, and suggests that in this case the waves transfer energy to the wind. This is referred to as the inverse Miles' mechanism. The use of u_λ and C_λ above eliminates the arbitrariness in choosing a reference level. It also reduces the number of governing parameters and is physically more meaningful because the thickness of the WBL decreases with frequency. The approximations (2.7) and (2.8) are also confirmed by Plant's (1982) data, including the quadratic dependence of β on $\breve{\omega}_a$ for $|\breve{\omega}_a| > 2$ (Fig. 1). The considerable scatter of Plant's data may be due to the additional dependence on C_λ.

Construction of a 1-D model of the WBL requires a definition of the vertical distribution of the wave-induced momentum flux τ in (2.1). For a monochromatic wave traveling at an angle θ to the wind, this is

$$\tau = \tau_o F(\varpi_a, C_\lambda, \xi), \tag{2.9}$$

where τ_o is the wave-induced momentum at the surface. The form of the scalar function F was investigated in numerical experiments with a 2-D model (Chalikov and Makin, 1991). An approximation based on the work of Makin (1989) is

$$F = [1 - \frac{\xi}{\xi_o}] e^{-10\xi} \tag{2.10}$$

where ξ_o is a function of the drag coefficient C_λ

$$\xi_o = 0.1 + 60 C_\lambda .$$

Thus, in practice F is independent of $\breve{\omega}_a$. The wave frequency influences the wave momentum flux at the surface, but not its vertical distribution. In the case of a multi-mode wave surface, it is assumed that τ is the superposition of the fluxes due to all spectral components.

The coefficient K_M in (2.2) may be computed from

$$K_M = Kz(e/c_1)^{1/2} \tag{2.11}$$

where c_1 is a constant equal to 4.6, and the turbulent kinetic energy e may be computed from

$$\frac{\partial e}{\partial t} = [K_M \frac{\partial \boldsymbol{u}}{\partial z} + \tau] \bullet \frac{\partial \boldsymbol{u}}{\partial z} - \frac{(e/c_1)^{3/2}}{Kz} . \qquad (2.12)$$

In (2.12) the effect of diffusion of turbulent kinetic energy is not included since it is usually small; the dot denotes the scalar product.

The model formulated above illustrates the general approach to be used when modelling the WBL-wave field system. The time and space evolution of the wave field may be simulated by a spectral wave model. The coupling of the two systems is accomplished through the exchange of information between the WBL and wave models. The WBL model computes and transfers to the wave model the spectral energy density input to the waves. The wave model computes the evolution of the wave spectrum in time and space and transfers the "sea state" to the WBL model. Equations (2.1) through (2.12) constitute a 3-D model describing the evolution of the atmosphere-wave coupling. These equations establish the connection between the turbulent stress and wind in the lowest layer of the atmosphere. The updated stress components are then used in the next time step.

The time scale T_s for the WBL processes may be estimated from

$$T_s = h/(\Delta C_z \, u) \ , \qquad (2.13)$$

where h is the thickness of the layer, and ΔC_z is the change in the drag coefficient due to the influence of the waves. Since ΔC_z is of the same order of magnitude as C_z, that is, $\Delta C_z \sim 10^{-3}$, T_s is on the order of 3×10^3s. The time step for a 3-D atmosphere model is on the same order of magnitude; therefore, it is reasonable to use the stationary version of the WBL equations:

$$\frac{\partial}{\partial z} (\boldsymbol{T}+\tau) = 0 \qquad (2.14)$$

$$[K_M \frac{\partial \boldsymbol{u}}{\partial z} + \tau] \bullet \frac{\partial \boldsymbol{u}}{\partial z} - \frac{K_M^3}{(Kz)^4} = 0 . \qquad (2.15)$$

Equation (2.14) may be written in the form:

$$\boldsymbol{T} + \tau = \boldsymbol{T}_h \ , \qquad (2.16)$$

where $\boldsymbol{T}_h$ is the constant of integration, which equals the stress vector above the WBL. Then (2.15) may be written:

$$\boldsymbol{T}_h \bullet \frac{\partial \boldsymbol{u}}{\partial z} - \frac{K_M^3}{(Kz)^4} = 0, \qquad (2.17)$$

which may be rewritten as

$$(Kz)^{4/3} \ (\boldsymbol{T}_h \bullet \frac{\partial \boldsymbol{u}}{\partial z})^{1/3} \ \frac{\partial \boldsymbol{u}}{\partial z} + \tau = \boldsymbol{T}_h. \qquad (2.18)$$

Since $\mathbf{T}_h$ is unknown, two boundary conditions are necessary to solve (2.18). The first is the prescribed velocity vector at height h,

$$z = h: \ \boldsymbol{u} = \boldsymbol{u}_h. \qquad (2.19)$$

The second is the expression for the tangential stress vector at the water surface,

$$z = z_r: \ K_M \frac{\partial \boldsymbol{u}}{\partial z} = \rho_a C_r \mid \boldsymbol{u}_r \mid \boldsymbol{u}_r \qquad (2.20)$$

The lower boundary height z_r is prescribed by the cut-off frequency ω_r:

$$z_r = \frac{2 \pi g}{\omega_r^2 \mid \cos \theta \mid}. \qquad (2.21)$$

It is assumed that the lowest part of the WBL is responsible for the creation of the local tangential stress due to waves with frequencies $\omega > \omega_r$. Waves with frequencies $\omega < \omega_r$ give rise to additional form drag which is taken into account in the integral (2.3). Assuming the Phillips' spectrum is valid for frequencies greater than ω_r:

$$\omega \geq \omega_r: \ S(\omega) = \alpha g^2 \omega^{-5} \qquad (2.22)$$

and that the local roughness ζ_o due to these waves is determined by their height, Chalikov and Belevich (1992) estimated

$$\zeta_o = \chi \alpha^{1/2} \frac{u_*^2}{g} \qquad (2.23)$$

with $\chi = 0.1$. Averaging the wave spectrum at $\omega=\omega_r$ over all angles:

$$S(\omega_r) = \frac{1}{2\pi} \int_{-\pi}^{\pi} S(\omega_r, \theta) \, d\theta \ , \qquad (2.24)$$

and equating this average to the Phillips' spectrum for $\omega = \omega_r$

$$S(\omega) = S(\omega_r)\left(\frac{\omega}{\omega_r}\right)^{-5} , \qquad (2.25)$$

(2.23) takes the form

$$\zeta_o = \chi \frac{u_*^2}{g^2} [S(\omega_r)]^{1/2} \omega_r^{5/2} . \qquad (2.26)$$

The local drag coefficient is then given by

$$C_r = [K/(\ln(z_r/\zeta_o))]^2 . \qquad (2.27)$$

An effective roughness parameter may then be found by combining (2.26) and the solution of (2.3). An approximation to this effective roughness is given in (2.31) below.

Equation (2.18), with boundary conditions (2.19), (2.20), and formulas (2.3) - (2.5), (2.7), (2.8), (2.10), (2.21), (2.26), and (2.27) formulate the parameterization of the WBL for use in coupling the atmosphere-wind wave system. Note that the integral in (2.3) depends on the vertical distribution of the wind u(z) and the drag coefficient C_z, which by definition is

$$C_z = | \boldsymbol{T}_b | / | \boldsymbol{u}(z) |^2 . \qquad (2.28)$$

For the numerical solution of (2.18) it is necessary to evaluate (2.3) by iteration. The values for C_z and u(z) may be obtained from a linear interpolation of the logarithmic scale

$$\xi' = \ln(z/z_r) ,$$

which, in practice, is convenient to use in the numerical solution of (2.18).

The approach presented above, although not overly complicated, takes a considerable amount of computer time. In the preliminary experiments discussed in this work, several simplifications were adopted: first, it was assumed that the spectra generated by the wave model includes the locally generated wind waves, which may be approximated by the JONSWAP spectrum (WAMDI group, 1988). The rest of the spectrum is considered to be swell and assumed not to contribute to the wave-induced momentum flux. This assumption, should not introduce large differences since the swell contribution to the wave induced momentum should be small due to the small steepness of these waves.

It was assumed that the spectral peak in the spectra generated by the wave model closest to the local wind corresponded to the locally generated wind sea. The frequency of this peak was determined by minimizing the expression

$$(k_{xi} - k_{xr})^2 + (k_{yi} - k_{yr})^2 \qquad (2.29)$$

where k_{xi}, k_{yi} are the x,y components of the wave number for spectral peak i, and k_{xr}, k_{yr} are those of the wave number of the shortest represented wave, which is assumed to be in the direction of the wind. Minimizing (2.29) is equivalent to minimizing

$$\omega_i^4 + \omega_r^4 - 2\omega_i^2\omega_r^2\cos(\theta_i - \theta_w) \qquad (2.30)$$

in frequency-direction space. ω_i and θ_i are the frequencies and directions of the different peaks, θ_w is the wind direction, and ω_r is the frequency of the shortest wave represented in the spectrum. Once the frequency of the local wind wave is selected, its corresponding phase speed is used to determine the inverse wave age, and the effective roughness height z_o is computed from

$$z_o = (u^2/g)\exp(-11.35+0.187R+(0.84+0.065R)(u/c_p))$$

with $R = \ln(u^2/(gz))$.

Equations (2.7) and (2.8), were not introduced. Only the large-scale coupling between the atmosphere and the waves has been, considered, hence equations (2.7) and (2.8), were not introduced.

3. SHEAR FLOW MECHANISM: JANSSEN'S APPROACH

The theory of wind generated gravity waves as presented by Miles (1957, 1960, 1976) is similar to the theory of the resonant interaction of plasma waves with particles (Landau and Lifshitz, 1954; Fabrikant, 1976). Surface waves in plane-parallel flow are generated with phase velocities equal to the wind velocity at some "critical" (or resonant) level, z_c. Depending upon the influence of the wave age on the Phillips' parameter in the wave spectrum, the wave-induced stress can be a significant fraction of the total stress (Janssen et al., 1989). For waves traveling along the mean horizontal wind **u**, and subject to certain conditions, Janssen (1982) has shown that the wind-wave interaction may be modeled by a diffusion-like coefficient, $D_w(k,z)$,

$$D_w(k,z) = \frac{\pi\omega^2 k}{C - V_g}\,\phi(k)\,|\chi(k,z)|^2. \qquad (3.1)$$

In the treatment that follows, vector notation will be dropped since it is assumed that the waves are aligned with the mean wind. Together with turbulent and viscous stress, the mean wind satisfies the equation,

$$\partial u/\partial t = \nu_a \frac{\partial^2 u}{\partial z^2} + \frac{1}{\rho_a}\frac{\partial T}{\partial z} + D_w(k,z)\frac{\partial^2 u}{\partial z^2} \qquad (3.2)$$

in which T is the turbulent stress which is assumed to be modeled by a mixing length theory.

In (3.1, 3.2), v_g, ϕ (k), ν_a, $D_w(k,z)$, and $\chi(k,z)$ denote: the group velocity of a surface wave with wave number k and phase speed c, the spectral amplitude, the molecular viscosity of air, the diffusion-like coefficient that models the air-sea interaction, and the normalized solution of the OSR equation, respectively.

The Orr-Sommerfeld equation is a 4^{th}-order ordinary differential equation:

$$\chi^{IV} - 2k^2\chi'' + k^4\chi = ikR_e[(u - c)(\chi'' - k^2\chi) - u''\chi] \qquad (3.3)$$

in which R_e is the Reynolds number. If R_e is taken to be infinite, then

$$\frac{d^2\chi}{dz^2} - k^2\chi - \frac{u''}{u - c}\chi = 0 , \qquad (3.4)$$

which is the OSR equation. For the MBL, the boundary conditions for (3.4) are

$$\chi\ (z \to 0) = 1$$

$$\chi\ (z \to \infty) = 0 \qquad (3.5)$$

The function $\chi(z,k)$ arises from a perturbation solution to a plane-parallel flow as follows. Let the nondimensional Navier-Stokes equation be expressed in terms of a mean and a perturbed flow:

$$p = P + p'$$

$$u = U + u' \qquad (3.6)$$

$$w = w'$$

$$u' = \frac{\partial \psi}{\partial z}$$

$$w' = -\frac{\partial \psi}{\partial x} \tag{3.7}$$

then

$$\frac{\partial^2 \psi}{\partial z \partial t} + U\frac{\partial^2 \psi}{\partial x \partial z} - \frac{\partial U}{\partial z}\frac{\partial \psi}{\partial x} = -\frac{\partial p'}{\partial x} + \frac{1}{R_e}\nabla^2\frac{\partial \psi}{\partial z} = 0$$

$$\frac{\partial^2 \psi}{\partial x \partial t} + U\frac{\partial^2 \psi}{\partial x^2} = \frac{\partial p'}{\partial z} + \frac{1}{R_e}\nabla^2\frac{\partial \psi}{\partial x} \tag{3.8}$$

where primes indicate perturbed quantities. Using the separation of variables technique with trial solutions

$$\psi(x,z,t) = \chi(z)\exp[ik(x-ct)]$$

$$p'(x,z,t) = \Pi(z)\exp[ik(x-ct)] \tag{3.9}$$

results in (3.10), and (3.11) below.

$$ik(U-c)\frac{d\chi}{dz} - ik\frac{dU}{dz}\chi = -ik\Pi + \frac{1}{R_e}\left(\frac{d^3\chi}{dz^3} - k^2\frac{d\chi}{dz}\right) \tag{3.10}$$

$$k^2(c-U)\chi = \frac{d\Pi}{dz} + \frac{ik}{R_e}\left(\frac{d^2\chi}{dz^2} - k^2\chi\right). \tag{3.11}$$

Equations (3.10) and (3.11) are a coupled system from which $\Pi(z)$ may be eliminated to get (3.3) and (3.4).

The Rayleigh equation, (3.4), has a singularity at the critical height, z_c. Since (3.6) - (3.11) are nondimensional, $\chi(z,k)$ is normalized. The steps used by Janssen to solve the preceding equations and estimate the wind-wave interaction are given schematically in Appendix A.

For a wave spectrum $\phi(k,\theta,t)$, Janssen (1991) gives the following

$$D_w(k,z) = \pi \int_{-\pi}^{\pi} d\theta \, \frac{\omega^2 k}{|\, c - v_g \,|} \, |\, \chi \,|^2 \, \phi(k,\theta,t) \cos^2\theta \quad (3.12)$$

in which θ is the angle between the wind and the spectral wave component.

A simplified version of Janssen's approach is used in this work. The simplification consists in deriving a generalized Charnock's constant as a function of wave age using Janssen's analysis. This generalized Charnock formula is then used to compute the roughness height z_o corresponding to the wave age μ as determined from the frequency f_p and wave number k_p of the "sea" spectral peak:

$$\mu = c_p/u_*, \; with \; c_p^2 = g/k_p.$$

This leads to a wave age dependent drag coefficient C_z.

This roughness height is passed from the wave model to the atmosphere model which then generates the winds which will drive the wave model for the next time step. In this fashion a two-way coupling between the wave and atmosphere models is achieved.

The generalized Charnock relation is derived from the family of curves adapted from Fig. 3 of Janssen (1989) (shown here in Fig. 2). These curves represent typical nondimensional velocity profiles with and without wave perturbed flow. In the figure the nondimensional velocity $u(z)/u_*$ is plotted versus the nondimensional height zg/u_*^2. The curves are nearly straight and parallel for $zg/u_*^2 > 1$. For $zg/u_*^2 < 1$ the perturbed curves deviate from log-linear, and, given boundary condition (A.3), cross the $u/u_* = 0$ intercept at $zg/u_*^2 = m = 0.0144$. The extrapolation is not shown in the figure.

Fig. 7 of Janssen (1989), shown here as Fig. 3, shows the dependence of C_z at a 10 m height on wave age for two values of u_* (0.3 m/s and 0.7 m/s). Curves are shown for both the -2/3 and the -3/2 power laws for the Phillips parameter (see Appendix A). It can be seen that there is considerable variation of C_z with wave age for the -3/2 power law. This power law was used in obtaining the curves in Janssen's Fig. 3.

The simplification used in this work was suggested by Fig. 2. For $zg/u_*^2 > 1$ the curves are merely displaced from the straight line representing the uncoupled wave-atmosphere situation. This suggests that a general equation for the family of curves may be written as:

$$u(z)/u_* = A \ln(zg/u_*^2) + B(\mu) \qquad (3.13)$$

where A is the slope of the family of curves, and B(μ) depends on wave age only. An average value of A is 2.46.

Equation (3.13) is rewritten as

$$u(z)/u_* = A \ln [zg/D(\mu)\, u_*^2] \qquad (3.14)$$

in which

$$B(\mu) = -A \ln[D(\mu)], \qquad (3.15)$$

thus,

$$C_z^{-1/2} = u(z)/u_* = A \ln[(1/C_z)\,(zg/D(\mu)\, u^2)]. \qquad (3.16)$$

In similar fashion the Charnock relation (1.3) may be written

$$C_z^{-1/2} = K^{-1} \ln[(1/C_z)\,(zg/m\, u^2)]. \qquad (3.17)$$

Comparing (3.16) and (3.17) suggests:

$$A = K^{-1}\ , \qquad (3.18)$$

and

D(μ) = a generalized Charnock "constant" (3.19)

which approaches m for large values of μ.

From (3.16) through (3.18), the generalized Charnock "constant" is:

$$D(\mu) = (zg/u^2)\,[C_z^{-1} \exp(-0.407 C_z^{-1/2})]\ . \qquad (3.20)$$

Computing the D(μ) for different values of wave ages yields

μ	5	10	15	20	25
D(μ)	0.210	0.727	0.414	0.0328	0.0277

.

A rational fraction that approximates D(μ) for $\mu > 3$ is given by

$$D(\mu) = (-0.153 - 0.00245\mu)/(1 - 0.358\mu) \qquad (3.21)$$

This approximation for $D(\mu)$ is used to generalize the Charnock relation:

$$z_o = D(\mu) \ (u_*^2/g) .$$

4. THE NMC ATMOSPHERE AND WAVE MODELS

Brief descriptions of the NMC atmosphere and ocean wave models are given below. Operationally these models run independently of each other, with the wave model using the output wind fields from the atmosphere model as the sole input. The operational wave model runs twice daily at the 0000 and 1200 UTC cycles. A so-called wave analysis is generated by running a 12-hour wave hindcast, that is, using the final analysis wind fields. This "wave analysis" provides the initialization wave field for a 72-hour forecast. The input wind field to the wave model is the lowest sigma layer winds reduced to a 10-m height assuming a logarithmic wind profile. For the coupling experiments the wave model was modified to take the u_* field directly from the atmosphere model. The runs were done once daily, for the 0000 UTC cycle only, thus initialization wave fields resulted from a 24 hour hindcast. The hindcast was done by running the NMC Global Data Assimilation System (GDAS) for the preceding 24 hours with the same coupling technique as for the forecasts.

4.1 The NMC atmosphere model

The operational NMC Medium Range Forecast Model (MRF) is used for the GDAS, the Aviation (3 day) forecast, and for the 10-day forecast runs. The MRF is a spectral model and is described in some detail in Kanamitsu (1989), and Kanamitsu et al. (1991). A few of its properties are described here.

The MRF forecast variables are vorticity, divergence, virtual temperature, specific humidity, and surface pressure. The model variables in the horizontal are represented by spherical harmonics. The model has 18 levels in the vertical and a horizontal resolution of triangular truncation 126 (T126). This truncation corresponds to a horizontal spatial resolution of approximately 105 km. However, in order to save computer time, the coupled atmosphere-wave experiments described here were performed with a triangular truncation of 62 (T62), which corresponds to a spatial resolution of approximately 210 km.

The lowest layer of the atmosphere model, the surface layer, is well defined with a height of 5 hPa (about 40 m) above the surface. The physics in this layer is governed by surface layer Monin-Obukhov similarity theory and improved land surface evaporation.

The atmospheric boundary layer (ABL) in the MRF consists of the bottom surface layer and those layers above it which are influenced

by the turbulent transfer of momentum, heat, and moisture from the surface layer. During vigorous daytime turbulent convection the ABL is typically 1 - 2 km thick. However, during extremely stable conditions, such as may occur at night, turbulence may become so weak and irregular that it may not be possible to determine accurately the height of the ABL. For these conditions, the ABL may recede into the surface boundary layer. The MRF makes no provision for this occurrence.

The MRF computes the surface turbulent fluxes of momentum, sensible heat, and latent heat. The heat fluxes are required for the solution of the heat balance equations that predict the air-ground interface temperature. This heat balance calculation is omitted over the oceans although it is important in predicting the evolution of the MBL. The surface fluxes of momentum and heat are used as boundary conditions for the diffusion equations which simulate the turbulent transfer of these quantities above the surface layer.

The calculation of surface fluxes in the MRF depends on the nondimensional variable z_s/L, where z_s is the height of the surface layer and L is the Monin-Obukhov length, the sign and magnitude of which determines the stratification/stability of the surface layer.

The vertical profiles of (virtual) potential temperature θ, specific humidity q, and wind speed in the surface layer are given by

$$\frac{\partial \theta}{\partial z} = \frac{\theta_*}{Kz}\,\varphi_T(z/L) \qquad (4.1)$$

$$\frac{\partial q}{\partial z} = \frac{q_*}{Kz}\,\varphi_q(z,L) \qquad (4.2)$$

$$\frac{\partial u}{\partial z} = \frac{u_*}{Kz}\,\varphi_U(z/L) \qquad (4.3)$$

with $L = \dfrac{\theta u_*^2}{Kg\theta_*}$.

θ_*, q_*, and u_* are the scaling factors for heat, moisture, and momentum. The functions $\varphi_{T,q,u}$ are the Obukhov functions which have been determined empirically.

Integration of the Obukhov functions leads to

$$z_s/L = (F_U^2/F_T)\, R_b, \tag{4.5}$$

in which R_b is the bulk Richardson number,

$$R_b = \frac{g z_s \Delta\theta}{\theta u_s^2}$$

and $F_{T,U,q}$ are the integrals of equations (4.1) - (4.3),

$$F_{T,U,q} = \int_{z_o}^{z_s} \frac{dz}{z}\, \varphi_{T,U,q}(z/L) \quad . \tag{4.6}$$

In these equations, $\Delta\theta$ is the difference in virtual potential temperature across the surface layer, Θ is the layer-average virtual potential temperature in the surface layer, u_s is the wind speed at the top of the layer, z_s, and z_o is the roughness height. In the current version of the MRF it is assumed that the roughness heights for momentum, heat, and moisture are equal. Over the ocean the roughness height z_o is taken as the form proposed by Charnock: (eq. 1.3), in which m is the Charnock constant (m=0.014).

Iterative solution of (4.5) using (4.6) yields values for z_s/L, u_*, θ_*, and q_*, and from these the surface fluxes F_M', F_T', F_q' are computed:

$$F_M' = -\rho_a u_*^2 = -\rho_a C_M(z_s, L)\, u_s^2 \quad , \tag{4.7}$$

$$F_T' = -\rho_a\, C_p\, u_*\, \theta_* = -\rho_a\, C_p\, C_T(z_s, L)\, u_s\, \Delta\theta \tag{4.8}$$

$$F_q' = -\rho_a\, \mathcal{L}\, u_*\, q_* = -\rho_a\, \mathcal{L}\, C_q(z_s, L)\, u_s\, \Delta q \tag{4.9}$$

C_M, C_T, and C_q are the drag (or transfer) coefficients for momentum, heat, and moisture respectively; $\mathcal{L}$ is the latent heat of vaporization, C_p is the specific heat of air, and Δq is the difference in specific humidity between z_s and z_o. Empirical data suggest that $C_T = C_q \approx C_M$. The MRF computes the transfer coefficients from

$$C_M = \left(\frac{u_*}{u_s}\right)^2 = \frac{K^2}{F_M^2} \qquad (4.10)$$

$$C_T = C_q = \frac{u_* \theta_*}{u_s \Delta \theta} = \frac{u_* q_*}{u_s \Delta q} = \frac{K^2}{F_M F_T} = \frac{K^2}{F_M F_q} \quad . \qquad (4.11)$$

For the special case of neutral static stability, the transfer coefficients become

$$C_M = C_T = C_q = \frac{K^2}{\ln^2(z_s/z_o)} \quad . \qquad (4.12)$$

4.2 The NMC global wave model

The operational NMC global ocean wave (NOW) model is a deep water spectral model with a 3 hour time step and a 2.5 by 2.5 degree latitude-longitude grid. It produces forecasts every 3 hours from 70°S to 75°N. The model solves at each grid point over the ocean the energy transport equation:

$$\frac{\partial S}{\partial t} + \boldsymbol{c_g} \cdot \nabla S = S_{in} + S_{nl}$$

where $S = S(f,\theta)$ is the two dimensional wave spectrum as a function of frequency f and direction θ, $\mathbf{c}_g$ is the group velocity, and the terms on the right-hand side are the source terms representing the wind input and the nonlinear wave-wave interactions.

The wind input source term follows the parameterization of Snyder et al. (1981), $S_{in} = \beta' \omega S$ with the wind wave growth parameter given by:

$$\beta' = \max[0, 3 \times 10^{-4}(30 u_* \omega g^{-1} \cos\theta - 1)] \quad , \qquad (4.13)$$

where ω is the radian wave frequency and θ is the angle between the wind and the wave directions.

The nonlinear source term is based on the SAIL II mechanism (Greenwood et al., 1985), and is given by

$$S_{nl} = \tfrac{1}{2} \phi \, C_z \, \omega^{-1} \, u_{10}^2 \qquad (4.14)$$

where ϕ is the Phillips' fetch constant ($0.8 \times 10^{-4} \leq \phi \leq 1.6 \times 10^{-4}$).

A $\cos^3 \theta$ law is used for spreading the energy over direction θ. Dissipation at high frequencies is accomplished by imposing the

Pierson-Moskowitz limit for a fully-developed spectrum (Pierson and Moskowitz, 1964).

The propagation scheme is a downstream interpolation in which each frequency-directional band is propagated at the group velocity along a great circle. Upwind swell is attenuated using an exponential attenuation term with maximum attenuation in the direction opposite to the local wind and decreasing angularly on either side to unity at 90 degrees.

5. COUPLING PROCEDURE

As indicated in sections 2 and 3 the procedure followed for coupling the two models was the same for the simplified Janssen (JS) and the Chalikov (CS) schemes.

To initialize the two-way coupling the 0000 UTC operational wave analysis and the GDAS u_* fields were used. The u_* field was transferred to the wave model and z_o values were computed using the given u_* field and the phase speeds from the wave spectra. The computed z_o field was transferred to the atmosphere model. Both models were then advanced 3 hours, the atmosphere model now using the wave age dependent z_o field in the Monin-Obukhov formulation. Starting with the next time step the wave model received a u_* field resulting from taking the wave age dependence into account. The procedure was then repeated. Every 24 hours a 120-hour wind forecast and a 120-hour wave forecast were started from the GDAS and wave hindcast fields. The exchange between the two models continued during the forecasts runs in the same fashion as for the hindcast (Fig. 4). The method for computing roughness over land remained unchanged.

In parallel with these runs the atmosphere and wave models were run without the two-way coupling, to serve as the control run. The resulting forecasts from the control and the coupled runs were compared.

The coupled runs using the JS approach for the nine consecutive days starting on December 26, 1991 are compared here with those using the CS approach for the eight consecutive days starting on January 24, in order to have about the same number of days using each approach.

6. RESULTS

Since the runs with the two approaches were done for different time periods, the results are not conclusive, for the synoptic conditions may have been different during the two periods. The effects of the coupling will depend on these conditions. As would be expected in the case of the waves, larger differences between the coupled and the control runs were observed in areas of strong winds where young seas would be expected. In the following two

sections typical results from both schemes will be given.

The impact on the waves was characterized by the difference in significant wave height (SWH) between the coupled and the corresponding control run. Impact on the wave spectra was also observed. However, the impact on the wave spectra could not be fully evaluated because spectra were saved at only a few locations around the continental United States.

6.1. IMPACT ON THE ATMOSPHERE MODEL

The largest impact on the atmosphere model during the model runs using the JS was for January 8th. Thus the results on this date will be discussed.

As can be seen from Figs. 5a and 5b, the JS increases the upward latent heat flux. The largest absolute difference between the two fields is approximately 73 watts/m^2 and is located off the northeastern coast of the United States. This location is also the site of the strongest upward sensible heat. A lesser difference was observed in the sensible heat fluxes (not shown). Thus it appears that the latent heat fluxes are more sensitive to the coupling than the sensible heat fluxes.

No impact was noticeable in either surface stress or the 10-m wind vectors. However, an increase in roughness height was observed over much of the ocean, as seen in Figs. 6a and 6b.

As will be discussed in section 6.2, the largest impacts on the surface ocean waves during the period January 24 to January 31 using the CS were observed for the forecasts starting on January 30th. Thus, the impact on the atmosphere model for this day will be discussed.

A slight decrease in the upward latent heat fluxes is noticed (Figs. 7a and 7b), while there is a slight increase in the upward sensible heat fluxes as well (Figs. 8a and 8b).

Larger differences are seen in the surface pressure forecasts, with a maximum decrease of approximately 2.9 hPa off the west coast of the United States, near the Canadian border. At this site the largest differences in the surface stresses, Fig. 9, and in 10 m winds, Fig. 10, are also noted. No roughness height fields are available for this case.

6.2 IMPACT ON THE WAVE MODEL

The effect of the coupling on the wave field will depend on the locations of active wave generation and on the pre-existing wave conditions. Since the two experiments were run for different time periods it is not possible to arrive at definite conclusions. However, the results presented in Tables 1 through 4 suggest that

the CS is more consistent and produces larger impact on the waves than the JS.

The tables give the distribution of differences in SWH between the coupled and control runs in different regions where the larger impacts were observed. Shown are the distribution of differences for successive 12-hour and 96-hour forecasts (the 120-hour forecasts could not be retrieved from the tape archive). A tendency for the range of differences to increase with time into the forecast can be seen.

For both approaches the impact of the coupling on the waves tends to increase with time (successive 12-hour and 96 hour forecasts) and with the forecast hour (12-hour forecasts versus 96-hour forecasts). The tendencies are more pronounced for the CS than for the JS.

The wave forecasts starting from 0000 UTC on January 30 are among the ones showing the larger impacts of the CS coupling. Figs. 11 a and b show contours of differences in SWH between the coupled and the control run for the 12-hour forecast in the North Pacific. The dashed contours indicate negative differences: coupled minus control. From Fig. 10 for the differences in the 10-m winds at 0000 UTC that day, it can been seen that the areas with reduced SWH's correspond approximately to areas with the larger differences in the 10-m winds. These areas are also those with the highest winds.

The 10-m winds are not available for 0000 UTC on February 3, 1992, but the difference contours of SWH for the 96-hour wave forecast valid at the time show significant differences off the northwest coast of the United States and Canada.

In contrast, the 10-m wind differences in the North Atlantic for 0000 UTC, January 30 are not as pronounced as those off the northwest U.S. and Canadian coast, and neither are the differences in SWH for the 12-hour forecast as seen in Fig. 11 b. The differences in SWH in the western area of the North Atlantic increased significantly for the 96-hour forecast (Fig. 12 b).

A slight increase of energy in the high frequencies and a broadening of the spectra were detected in the directional spectra for the coupled runs. Slight changes of a few degrees were noticed in the wind direction. These changes in wind direction appear to have an effect on the spectra for the coupled runs.

One location where spectra were saved and where significant differences in SWH occurred was at 45°N-130°W. Figs. 13a and b show the directional and frequency spectra at this location for the 96-hour forecasts valid at 0000 UTC on February 3, 1992. Fig. 13a shows the spectra for the control run and 13b for the CS run. The coupling reduced the SWH by 1.5 m, the u_* by 0.11 m/s, and there

was a change in wind direction of 6.7 degrees. The directional spectra show a change in the location of the spectral peak along with a broadening and flattening of the spectrum. The spectral peak is better aligned with the wind direction. It is noted that the wave model often overpredicts the SWH in this region. The CS in general reduced the SWH, which appears to be a step in the right direction.

7. DISCUSSION

The two methods presented here are conceptually different. The Chalikov approach proceeds from numerical solutions of the equations of motion and numerical computations of the vertical fluxes due to turbulence and wave induced perturbations; the Janssen approach is posed as a classical instability problem.

Simplifications have been made to both these approaches in applying them to couple the two models. These simplifications may in part be responsible for the small impacts obtained.

From the tables and figures given here it can be seen that the impact of the coupling for both methods is noticeable only in small areas of high wind speeds. This alone may be significant, especially when considering hurricane/typhoon models.

It is noted that the Chalikov approach in general reduced wave heights thus increased the roughness height. On the other hand for the Janssen case, the occurrence of increased wave heights was higher than that of decreased wave heights.

A more sophisticated treatment whereby the wave-generated momentum flux is transferred to the atmosphere model may be more revealing. Continuation of the experiment for a longer time period especially during the southern hemisphere winter would be desirable.

Acknowledgements. The authors wish to express their thanks to Rachel Teboulle for developing the graphics and for helping with the compilation of statistics between the coupled and control runs. Their thanks also go to Hann-Ming Juang and Masao Kanamitsu for their help.

APPENDIX A

In order to solve the Rayleigh equation coupled with a diffusion-like equation and to estimate the wind-wave interaction, Janssen used the following steps:

a. Assume the unperturbed wind profile is

$$u(z) = \left(\frac{u_*}{Kz}\right) \ln\left(\frac{z}{z_o}\right) . \qquad (A.1)$$

b. Solve (3.4) with boundary conditions (3.5) for a given $k = \omega^2/g$.

c. Construct an extended diffusion-like equation:

$$\frac{\partial u}{\partial t} = \frac{\partial}{\partial z}\left(K^2 z^2 \left|\frac{\partial u}{\partial z}\right| \frac{\partial u}{\partial z}\right) + \left[\nu_a + D_w(k,z)\right] \frac{\partial^2 u}{\partial z^2} \qquad (A.2)$$

where the mixing length hypothesis is used for the turbulent diffusion.

d. Solve (A.2) as an initial value problem with boundary conditions:

$$u(z=z_o, t) = 0 \quad ; \quad z_o = (m/g)\, u_*^2, \qquad (A.3)$$

where the expression for z_o is the Charnock relation (1955), and

$$\lim_{z \to \infty} K^2 z^2 \left|\frac{\partial u}{\partial z}\right| \frac{\partial u}{\partial z} = u_*^2 \qquad (A.4)$$

until u(z,t) reaches a steady state.

e. Repeat steps a-d iteratively until u(z,t) and D_w do not change substantially.

The wave induced stress is then computed from:

$$\tau_w(z=0) = -\rho_a \int_o^\infty dz D_w(k,z) \frac{\partial^2 u}{\partial z^2} . \qquad (A.5)$$

On the basis of wave breaking and dimensional grounds, Phillips (1958) proposed the spectral form

$$\phi(k) = \frac{1}{2}\,\alpha_p k^{-4} \quad k \geq k_p$$

$$\phi(k) = o \qquad k < k_p \tag{A.6}$$

where α_p is Phillips' parameter or "constant", and k_p is the wave number of the spectral peak. For the spectrum ϕ in (3.1), Janssen assumed the JONSWAP mean spectrum for a growing sea, (Hasselmann et al., 1973):

$$\phi(k) = \frac{1}{2}\alpha_p\, k^{-3} \exp\left[-\frac{5}{4}\left(\frac{k_p}{k}\right)^2\right] \gamma^r \tag{A.7}$$

$$r = \exp -\frac{1}{2}\left[(k^{1/2} - k_p^{1/2})/\sigma\, k_p^{1/2}\right]^2 \tag{A.8}$$

where $\gamma = 3.3$, and $\sigma = 0.1$.

Empirical data suggest that the Phillips' parameter depends on wave age. Based on some field and laboratory data, Snyder (1974) proposed:

$$\alpha_p = b_1 \left(\frac{c_p}{u_*}\right)^{-2/3} , \tag{A.9}$$

with b_1 a constant. Janssen showed that this form yields a wave induced stress nearly independent of wave age. A better fit to field data is given by

$$\alpha_p = 0.57 \left(\frac{c_p}{u_*}\right)^{-3/2} , \tag{A.10}$$

(Janssen et al., 1984). Using this power law, Janssen found a fairly pronounced dependence of wave-induced stress on wave age.

APPENDIX B

For completeness, an approximate solution to (3.16, 3.17) is given here. Let us define the generalized Froude numbers, Fr:

$$Fr = D(\mu)\,(u^2/zg) \quad or \quad mu^2/zg \tag{B.1}$$

so that

$$C_M^{1/2} = -K/ln(C_M Fr) \ . \tag{B.2}$$

C_M is an implicit function of Fr; given Fr, C_M can be computed by iteration. A more direct approach is to compute C_M for several widely separated values of Fr and then to use an interpolation approximation such as,

$$C_M(Fr) \cong [(6.283 + 0.2077\ x)/(1-0.6448x)]x10^{-3} \tag{B.3}$$

where x = lnFr, and $-13.4 < x < 0.94$.

Another approximation is suggested by (3.17). Let C_M be approximated on the right-hand-side of (3.17) by a constant C_o. Then,

$$C_M \cong \frac{K^2}{(\ln Fr + lnC_o)^2} \tag{B.4}$$

which suggests

$$C_M \cong [a_o/(1 + b_1 x + b_2 x^2)]x10^{-3} \tag{B.5}$$

where as before, x = lnFr. The result is

$$C_M \cong (6.64\ x\ 10^{-3})/(1 - 0.677x + 0.0456x^2) \ , \tag{B.6}$$

which works about as well as (B.3).

References

Burgers, G. and V. Makin, 1992: Boundary layer model results for wind-sea growth. J. Phys. Oceanog. (in press).

Chalikov, D., 1976: A mathematical model of wind-induced waves. Dokl. Akad. Nauk SSSR, **229**, 1083.

Chalikov, D., 1978: The numerical simulation of wind-wave interaction. J. Fluid Mech., **87**, 561-582.

Chalikov, D., 1986: Numerical simulation of the boundary layer above waves. Bound.-Layer Met., **24**, 63-98.

Chalikov, D., 1992: Comments on "Wave Induced Stress and the Drag of Air Flow over Sea Waves" and "Quasi-linear Theory of Wind Wave Generation Applied to Wave Forecasting". (Submitted to J. Phys. Oceanogr).

Chalikov, D., and V. Makin, 1991: Models of the wave boundary layer. Bound.-Layer Meteor., **56**, 83-99.

Chalikov, D.V., and M. Yu Belevich, 1992: One-dimensional theory of the wave boundary layer. Bound.-Layer Met. (In press)

Charnock, H., 1955: Wind stress on a water surface. Quart. J. Roy. Meteorol. Soc., **81**, 639-640.

Donelan, M.A., 1982: The dependence of the aerodynamic drag coefficient on wave parameters. Proc. First Int. Conf. on Meteor. and Air-Sea Interaction of the Coastal Zone. The Hague, Amer. Meteor. Soc., 381-387.

Fabrikant, A.L., 1976: Quasilinear theory of wind-wave generation. Izv. Acad. Sci. USSR, Atmos. Ocean Phys., **12**, 524-526.

Hasselmann, K., T.P. Barnett, E. Bouws, H. Carlson, D.E. Cartwright, K. Enke, J.A. Ewing, H. Gienapp, D.E. Hasselmann, P. Kruseman, A. Meerburg, P. Muller, P.D.J. Olbers, K. Richter, W. Sell, and H. Walden, 1973: Measurement of wind-wave growth and swell decay during the Joint Sea Wave Project (JONSWAP). Dtsch. Hydr. Z., Suppl. A, **80**, (12) 1-95.

Hsiao, S.V., and O.H. Shemdin, 1983: Measurements of wind velocity and pressure with a wave follower during MARSEN. J. Geophys. Res. **88** (C14), 9841-9849.

Garratt, J.R., 1977: Review of the drag coefficient over oceans and continent. Mon. Wea. Rev., **105**, 915-929.

Greenwood, J.A., V.J. Cardone, and L.M. Larson, 1985: Chapter 22, The Swamp Group, Ocean Wave Modeling. Plenum Press, 256 pp.

Janssen, P.A.E.M., 1989: Wind-induced stress and the drag of air flow over sea waves. J. Phys. Oceanogr., **19**, 745-754.

Janssen, P.A.E.M., 1991: Quasi-linear theory of wind-wave generation applied to wave forecasting. J. Phys. Oceanog., **21**, 1631-1642.

Janssen, P.A.E.M, G.J. Komen, and W.J.P. de Voogt, 1984: An operational coupled hybrid wave prediction model. J. Geophys. Res., **89**, 3635-3654.

Janssen, P.A.E.M., G.J. Komen and W.J.P. de Voogt, 1984: An operational coupled hybrid wave prediction model. J. Geophys. Res., 89, 3635-3654.

Janssen, P.A.E.M., P. Lionello, and W. Zambreski, 1989: On the interaction of wind and waves. Phil. Trans. R. Soc. London, **A329**, 289-301.

Janssen, P.A.E.M., 1982: Quasilinear approximation for the spectrum of wind-generated water waves. J. Fluid Mech., **117**, 493-506.

Jeffreys, H., 1925: On the formation of water waves by wind. Proc. Roy. Soc. **A 107**(A742) 189-206.

Kanamitsu, M., 1989: Description of the NMC global data assimilation and forecast system, Weather and Forecasting, **4**, 335-342.

Kanamitsu, M., J.C. Alpert, K.A. Campana, P.M. Caplan, D.G. Deaven, M. Iredell, B. Katz, H.-L. Pan, J. Sela and G.H. White, 1991: Recent changes implemented into the global forecast system at NMC. Weather and Forecasting, **6**, 425-435.

Kitaigorodski, S.A, 1968: On the calculation of the aerodynamics roughness of the sea surface. Izv. Atmos. Oceanic Phys. **4**, 498-502.

Landau, L.D. and E.M. Lifshitz, 1954: Electrodynamics of continuous media. Pergamon Press, 536 pp.

Makin, V., 1989: The dynamics and structure of the boundary layer above sea. Senior doctorate thesis. Inst. of Oceanology, Acad. of Sci. of the USSR, Moscow, 417 pp (in Russian).

Miles, John W., 1957: On the generation of surface waves by shear flows. Jour. Fluid Mech. **3**(2) 185-204.

Miles, John W., 1960: On the generation of surface waves by turbulent shear flows. Jour. Fluid Mech. 7(3) 469-478.

Miles, J.W., 1976: Nonlinear surface waves in closed basins. J. Fluid Mech., 75, 419-448.

Orr, W. McF., 1907: The stability or instability of the steady motion of a liquid. Proc. Royal Irish Acad. A, 27, 69-138.

Phillips, O.M., 1957: On the generation of waves by turbulent wind. Jour. Fluid Mech. 2(5) 417-445.

Pierson, W.J. and L. Moskowitz, 1964: A proposed spectral form for a fully developed wind sea based on the similarity theory of S. Kitaigorodskii. J. Geophys. Res., 69, 5181-5190.

Plant, W.J., 1982. A relationship between wind stress and wave slope. J. Geophys. Res., 87 (C3), 1961-1967.

Rayleigh, Lord, 1880: On the stability, or instability, of certain fluid motions. Scientific papers 1, Cambridge Univ. Press, 474-487.

Roeckner, E., L. Dumenil, E. Kirk, F. Lunkeit, M. Ponater, B. Rockel, R. Sausen, U. Schlese, 1989: The Hamburg version of the ECMWF model (ECHAM). GARP Report 13, WMO Geneva, WMO/TP 332 pp.

Snyder, R.L., 1974: A field study of wave-induced pressure fluctuation above surface gravity waves. J. Mar. Res., 32, 497-531.

Snyder, R.L., F.W. Dobson, J.A. Elliot, and R.B. Long, 1981: Array measurements of atmospheric pressure fluctuations above gravity waves. J. Fluid Mech., 102, 1-59.

Sommerfeld, A., 1908: Ein beitrag zur hydrodynamischen erklarung der turbulenten flussigkeits bewegung. Pro. 4th Int. Congr. Math. Rome, 116-124

Stewart, R.W., 1967: Mechanics of the air-sea interface. Phys. Fluid Suppl., 10, S 47-53.

WAMDI Group (Hasselmann, S., K. Hasselmann, E. Banner, P.A.E.M. Janssen, G. J. Komen, L. Bertotti, P. Lionello, A. Guillaume, V.J. Cardone, J.A. Greenwood, M.Reistad, L. Zambresky, and J.A. Ewing), 1988. The WAM model-A third generation ocean wave prediction model. J. Phys. Oceanogr., 18, 1775-1810.

Weber, S.L., H. von Storch, P. Viterbo, and L. Zambresky, 1991: Coupling an ocean wave model to an atmospheric general circulation model. Max-Planck-Institute fur Meteorologie, Report N. 72, Hamburg.

Table 1a. Distribution of differences in SWH between the coupled Chalikov (CS) and the control runs for successive twelve-hour forecasts. The northeast Pacific has 534 grid points. The percentages of grid points in the region with SWH differences within the indicated intervals are given.

	Percentage of Grid Points							
Day Number	1	2	3	4	5	6	7	8
SWH Dif. (m)								
-1.25--1.00			0.2	0.5				
-1.00--0.75			0.6	1.1	0.2		1.3	
-0.75--0.50	0.2	0.4	0.7	1.7	4.3		8.6	
-0.50--0.25	3.0	4.7	4.7	6.2	13.3	10.3	29.2	
-0.25- 0.25	96.8	94.9	93.8	89.0	81.3	89.7	54.1	
0.25- 0.50				0.6	0.9		2.6	
0.50- 0.75							1.7	
0.75- 1.00				0.6			1.5	
1.00- 1.25				0.3			0.4	
1.25- 1.50							0.6	
Total	100.0	100.0	100.0	100.0	100.0	100.0	100.0	

Table 1b. Same as Table 1a for the ninety-six-hour forecasts.

	Percentage Grid Points							
Day Number	1	2	3	4	5	6	7	8
SWH Dif (m)								
-2.50--2.25		0.6						
-2.25--2.00		0.4						
-2.00--1.75		0.7					0.6	
-1.75--1.50		0.6					1.3	
-1.50--1.25		0.9	0.6				2.2	
-1.25--1.00		0.9	0.4				2.2	0.2
-1.00--0.75	0.2	0.9	1.3				2.1	0.2
-0.75--0.50	0.9	1.9	3.0			1.1	3.0	0.7
-0.50--0.25	8.4	4.5	8.8	9.6		3.2	6.2	9.0
-0.25- 0.25	88.4	85.0	85.0	86.0		92.7	72.7	87.6
0.25- 0.50	1.5	2.8	0.7	3.2		1.7	8.6	2.2
0.50- 0.75	0.2	0.9	0.2	1.0		0.9	1.1	
0.75- 1.00		0.6		0.2				
1.00- 1.25	0.2					0.4		
1.25- 1.50		0.2						
Total	99.8	99.9	100.0	100.0		100.0	100.0	99.9

Table 2a. Twelve-hour forecast for successive days using CS approach. The northwest Atlantic has 274 grid points.

	Percentage Grid Points							
Day Number SWH Dif (m)	1	2	3	4	5	6	7	8
-1.00--0.75	0.3							
-0.75--0.50	1.7							0.3
-0.50--0.25	2.4	4.5	2.1	0.4		2.8		8.0
-0.25- 0.25	95.5	95.5	97.9	98.6		97.2	100.0	62.6
0.25- 0.50				1.0				12.1
0.50- 0.75								10.7
0.75- 1.00								3.8
1.00- 1.25								2.4
Total	99.9	100.0	100.0	100.0		100.0	100.0	99.9

Table 2b. Same as Table 2a for the 96-hour forecasts.

	Percentage Grid Points							
Day Number	1	2	3	4	5	6	7	8
SWH Dif (m)								
-1.50--1.25					0.3			
-1.25--1.00			0.3		1.4	0.3	5.5	
-1.00--0.75			0.7	0.3	4.5	1.0	5.5	1.7
-0.75--0.50			3.1	1.7	24.5	3.1	10.7	2.8
-0.50--0.25			5.2	4.5	21.4	8.0	22.5	14.9
-0.25- 0.25	100.0	100.0	85.8	89.3	45.9	70.9	54.0	76.1
0.25- 0.50			4.8	3.5	1.7	10.7	1.4	4.5
0.50- 0.75				0.7	0.3	4.5	0.3	
Total	100.0	100.0	99.9	99.8	99.1	89.4	100.0	100.0

Table 3a. Distribution of SWH differences between the Janssen (JS) and the control run. Successive twelve-hour forecasts for the northeast Pacific with 534 grid points. The percentage of grid points in the region with SWH difference within the indicated interval are given.

	Percentage Grid Points								
Day Number SWH Dif. (m)	1	2	3	4	5	6	7	8	9
-0.75--0.50						0.4		0.7	
-0.50--0.25	0.6	0.7				0.2		1.5	1.9
-0.25- 0.25	97.9	94.8	98.9	100.0	99.8	97.2	96.8	95.3	95.1
0.25- 0.50	1.5	4.5	1.1		0.2	1.9	3.0	2.4	1.9
0.50- 0.75						0.4	0.2		0.2
Total	100.0	100.0	100.0	100.0	100.0	100.1	100.0	99.9	99.1

Table 3b. Same as Table 3a for the 96-hour forecasts.

Percentage Grid Points

Day Number SWH Dif. (m)	1	2	3	4	5	6	7	8	9
-1.25--1.00							0.4		
-1.00--0.75	0.4		0.2				0.2	0.2	
-0.75--0.50	0.2		1.1				0.7	1.3	2.2
-0.50--0.25	0.7	0.9	2.1	6.7		0.2	4.7	4.7	8.0
-0.25- 0.25	85.4	95.1	92.0	91.6	81.7	92.0	84.7	84.5	85.8
0.25- 0.50	8.0	3.7	3.0	1.5	14.2	6.4	7.1	5.4	3.9
0.50- 0.75	4.5	0.2	1.5	0.2	4.1	1.4	1.7	2.4	
0.75- 1.00	0.7						0.2	0.9	
1.00- 1.25							0.3	0.6	
Total	98.6	99.9	99.9	100.0	100.0	100.0	100.0	100.0	99.9

Table 4a. Same as Table 3a for the northwest Atlantic

	Percentage Grid Points								
Day Number SWH Dif. (m)	1	2	3	4	5	6	7	8	9
-0.25-0.25	98.9	98.9	96.0	100.0	96.0	96.0	99.3	90.9	98.9
0.25- 0.50	1.1	1.1	4.0		3.6	4.0	0.7	9.1	1.1
-									
Total	100.0	100.0	100.0	100.0	99.6	100.0	100.0	100.0	100.0

Table 4b. Same as Table 3b for the northwest Atlantic.

Day Number SWH Dif. (m)	Percentage Grid Points 1	2	3	4	5	6	7	8	9
-1.00--0.75							0.7		
-0.75--0.50	0.3				0.3		1.0		
-0.50--0.25	2.4	1.0	0.3		2.4	1.7	3.7	1.0	1.4
-0.25- 0.25	94.1	94.1	92.4	95.2	94.8	91.0	93.2	79.6	89.1
0.25- 0.50	3.1	4.5	6.9	4.8	2.4	6.6	1.0	13.3	8.8
0.50- 0.75		0.3	0.3			0.7	0.3	3.1	0.7
0.75- 1.00								1.0	
1.00- 1.25								1.0	
1.25- 1.50								0.7	
1.50- 1.75									
1.75- 2.00								0.3	
Total	99.9	99.9	99.9	100.0	99.9	100.0	99.9	99.7	100.0

FIGURE CAPTIONS.

Fig. 1. Wave growth parameter vs inverse wave age for different values of the drag coefficient. Markers: Plant's data; solid lines: approximation from equations (2.7) and (2.8).

Fig. 2. Adaptation of Fig. 3 from Janssen (1989). Dimensionless wind speed as a function of dimensionless height for $u_* = 0.7$ m/s. The thin line represents $\mu \to \infty$.

Fig. 3. Reproduction of Fig. 7 from Janssen (1989). Aerodynamic drag over sea waves as a function of wave age for two different parameterizations of Phillips' constant.

Fig. 4. The coupling procedure. Downward arrows indicate transfer of u_* from the atmospheric model to the wave model, and upward arrows indicate transfer of z_0 from the global wave model to the atmosphere model. The "hindcast" continues for all the days of the experiment. Every 24 hours at 0000 UTC a 120-hour wave forecast is initiated.

Fig. 5a. Contour plot of surface latent heat flux for the 24-hour forecast of the control run for 0000 UTC, January 8, 1992.

Fig. 5b. Same as 5a for the JS run.

Fig. 6a. Contours of roughness height (z_0) for the control run of January 8, 1992.

Fig. 6b. Same as Fig. 6a for the JS run.

Fig. 7a. Same as Fig. 5a for January 30, 1992.

Fig. 7b. Same as Fig. 5b for January 30, 1992, CS run.

Fig. 8. Contours of surface heat flux for the January 8, 1992 control run.

Fig. 8b. Same as Fig. 8a for the JS run.

Fig. 9. Vector differences in the surface stresses between the CS and control runs for 0000 UTC January 30, 1992.

Fig. 10. Same as Fig. 9 for the 10-m height winds.

Fig. 11a. Contours of differences in SWH between the CS run and the control run: coupled minus control. North Pacific for the 12-hour forecast valid 1200 UTC January 30, 1992. Solid contours indicate positive differences, dashed contours indicate negative differences. Contour lines over land should be disregarded.

Fig. 11b. Same as Fig. 11a for the north Atlantic.

Fig. 12a. Same as Fig. 11a for the 96-hour forecast valid February 3, 1992.

Fig. 12b. Same as Fig. 11b for the 96-hour forecast valid February, 2, 1992.

Fig. 13a. Forecast directional and frequency wave spectra at grid point located at 45°N -130°W for the 96-hour forecast valid 0000 UTC February 3, 1992 for the control run. Arrow on the margin of the directional spectrum indicates u_*. Spectral densities are normalized relative to the maximum spectral density.

Fig. 13b. Same as Fig. 13a for the CS run.

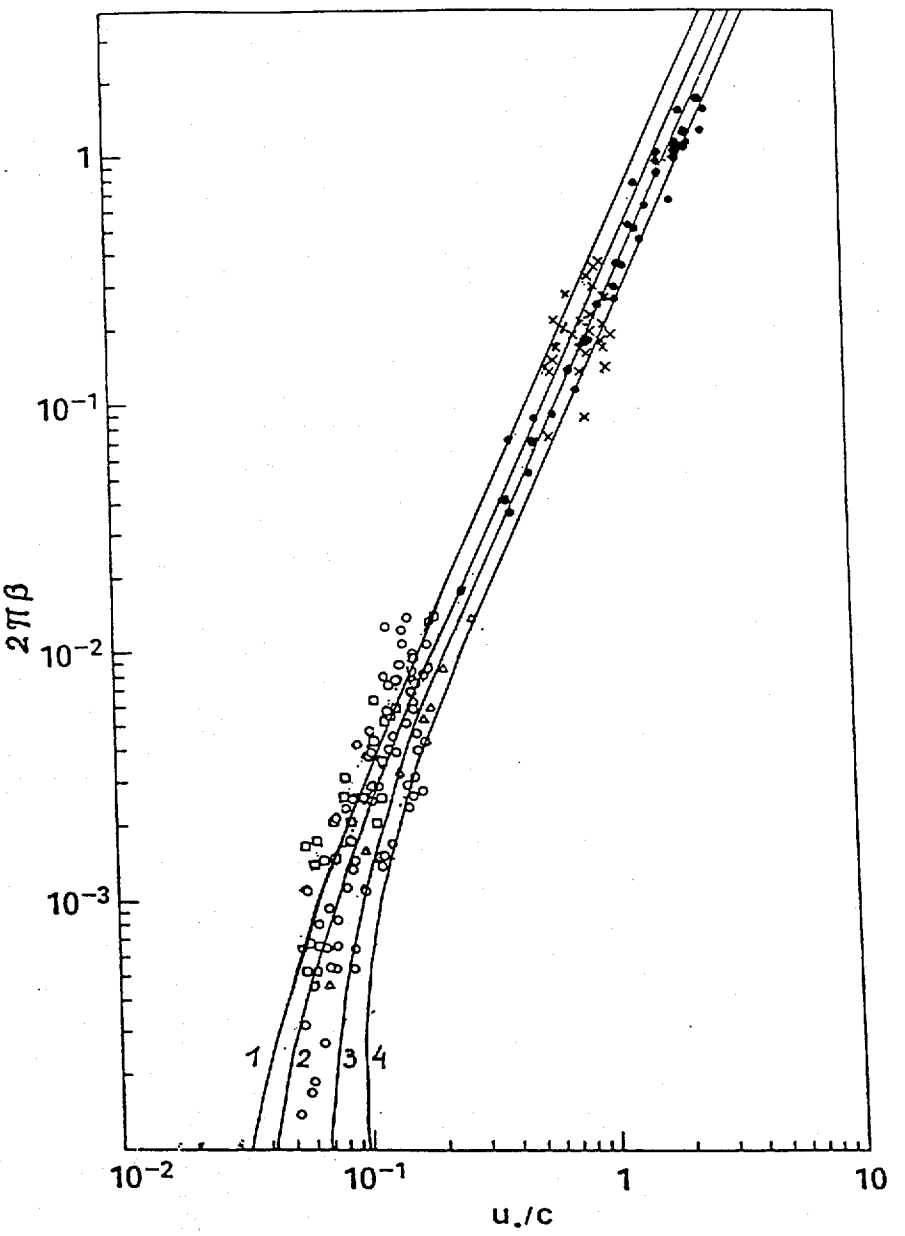

Figure 1.

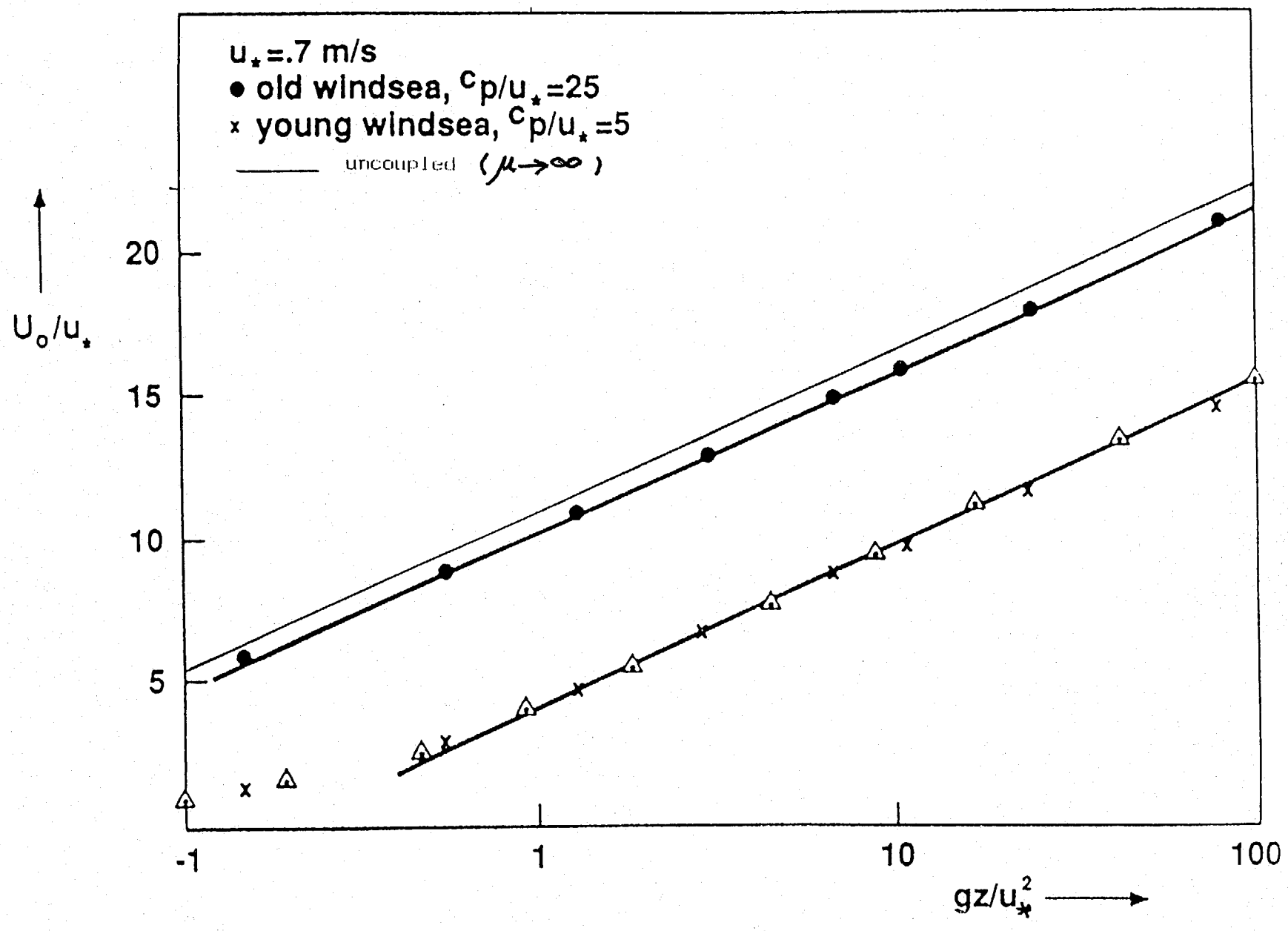
u_*=.7 m/s
● old windsea, $^cp/u_*$=25
x young windsea, $^cp/u_*$=5
uncoupled ($\mu \to \infty$)
U_o/u_*
20
15
10
5
-1
1
10
100
gz/u_*^2

Figure 2.

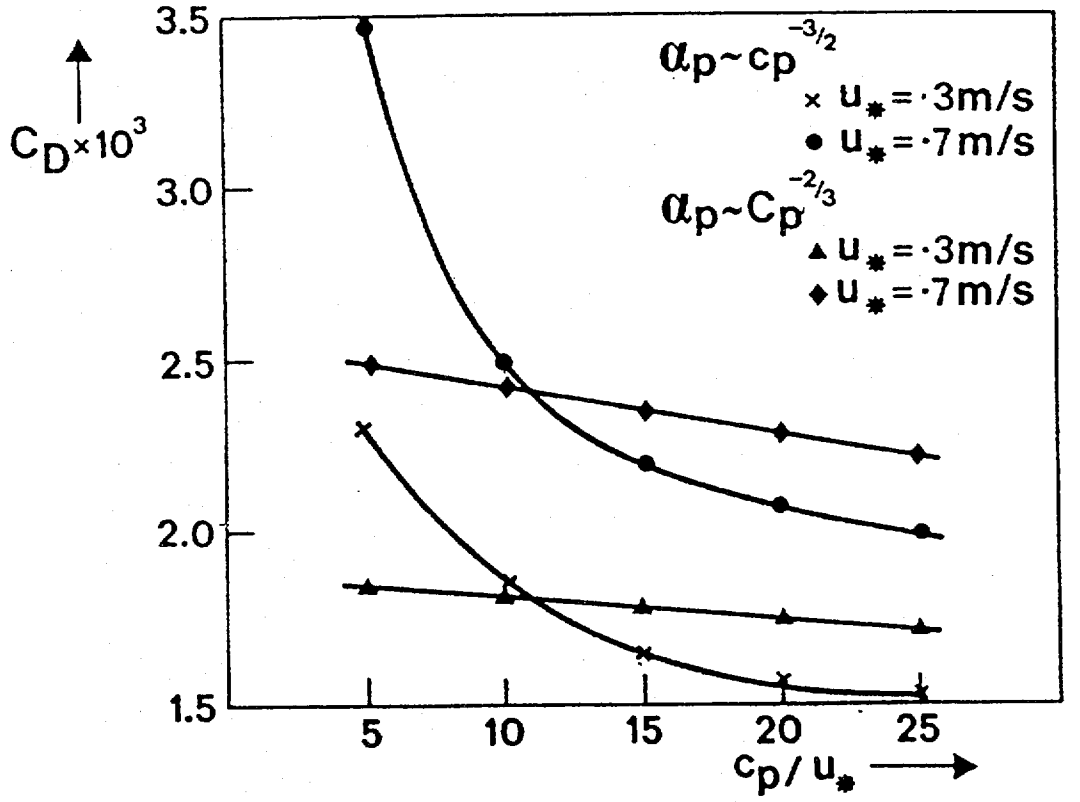
3.5
3.0
2.5
2.0
1.5
$C_D \times 10^3$
$\alpha_p \sim cp^{-3/2}$
× $u_* = \cdot 3$m/s
● $u_* = \cdot 7$m/s
$\alpha_p \sim Cp^{-2/3}$
▲ $u_* = \cdot 3$m/s
◆ $u_* = \cdot 7$m/s
5
10
15
20
25
c_p / u_*

Figure 3.

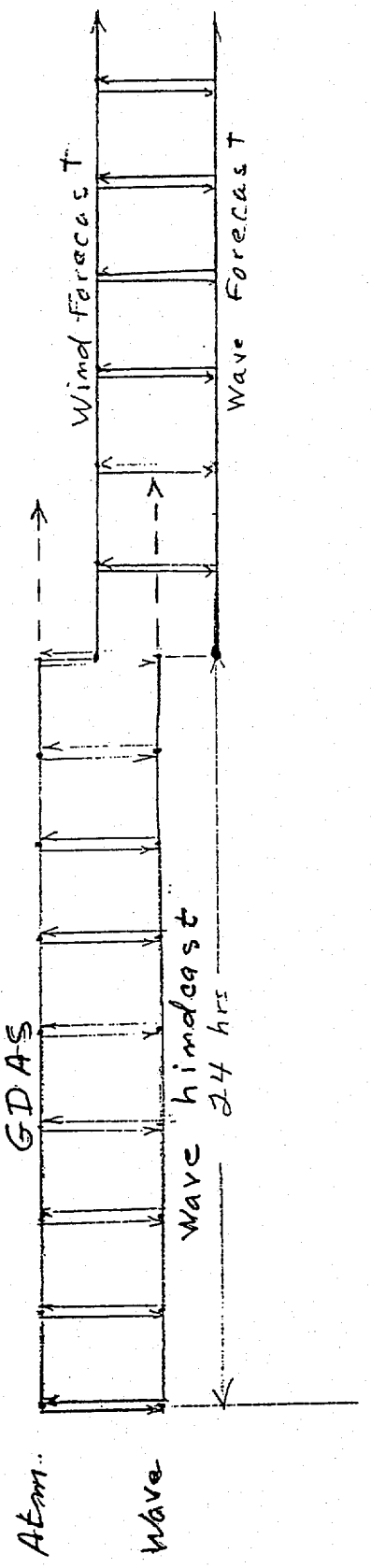
Wind Forecast
Wave Forecast
GDAS
Wave hindcast
24 hrs
Atm.
Wave

Figure 4.

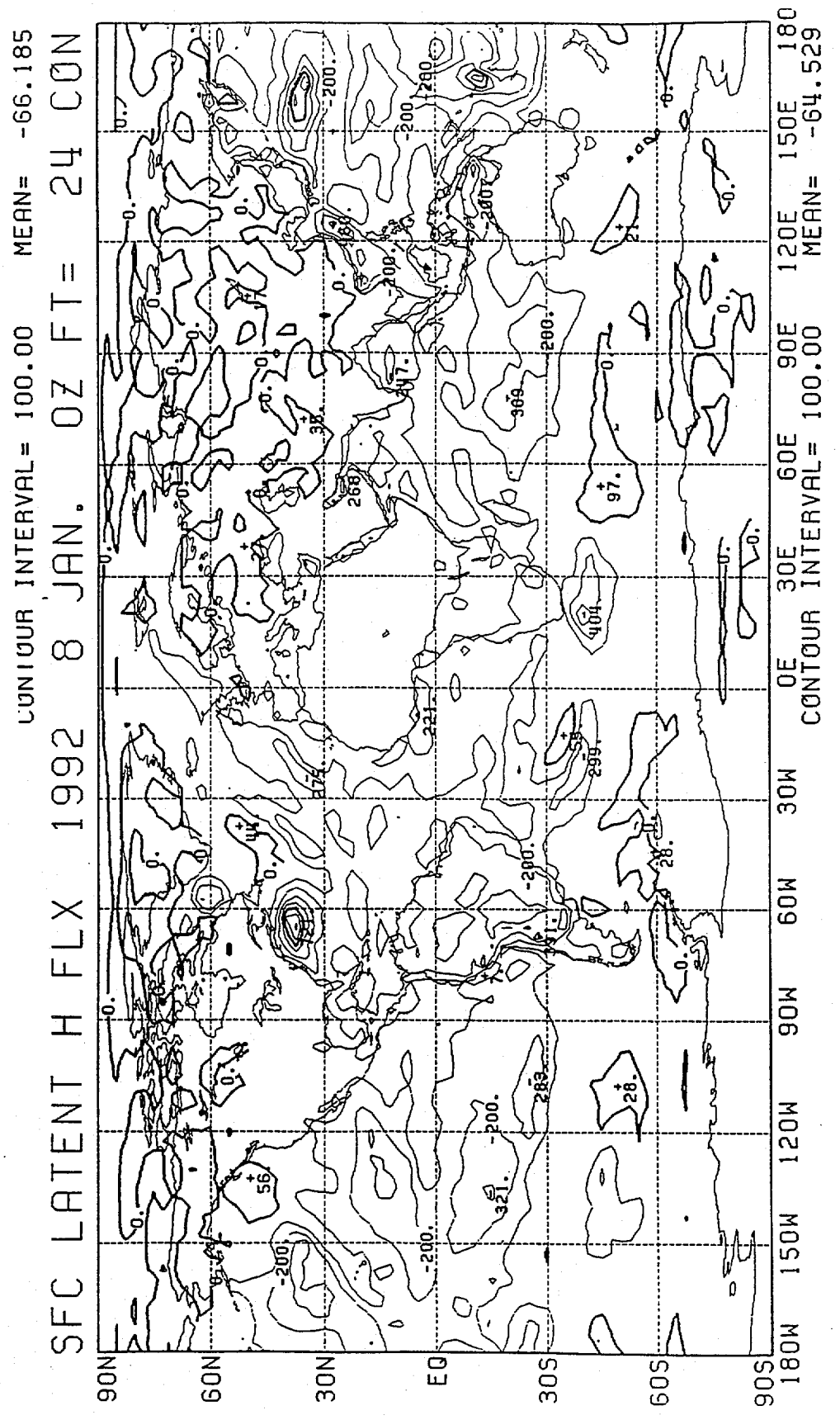
SFC LATENT H FLX 1992 8 JAN. 0Z FT= 24 CON
CONTOUR INTERVAL= 100.00 MEAN= -66.185
CONTOUR INTERVAL= 100.00 MEAN= -64.529
90N
60N
30N
EQ
30S
60S
90S
180W
150W
120W
90W
60W
30W
0E
30E
60E
90E
120E
150E
180

Figure 5a.

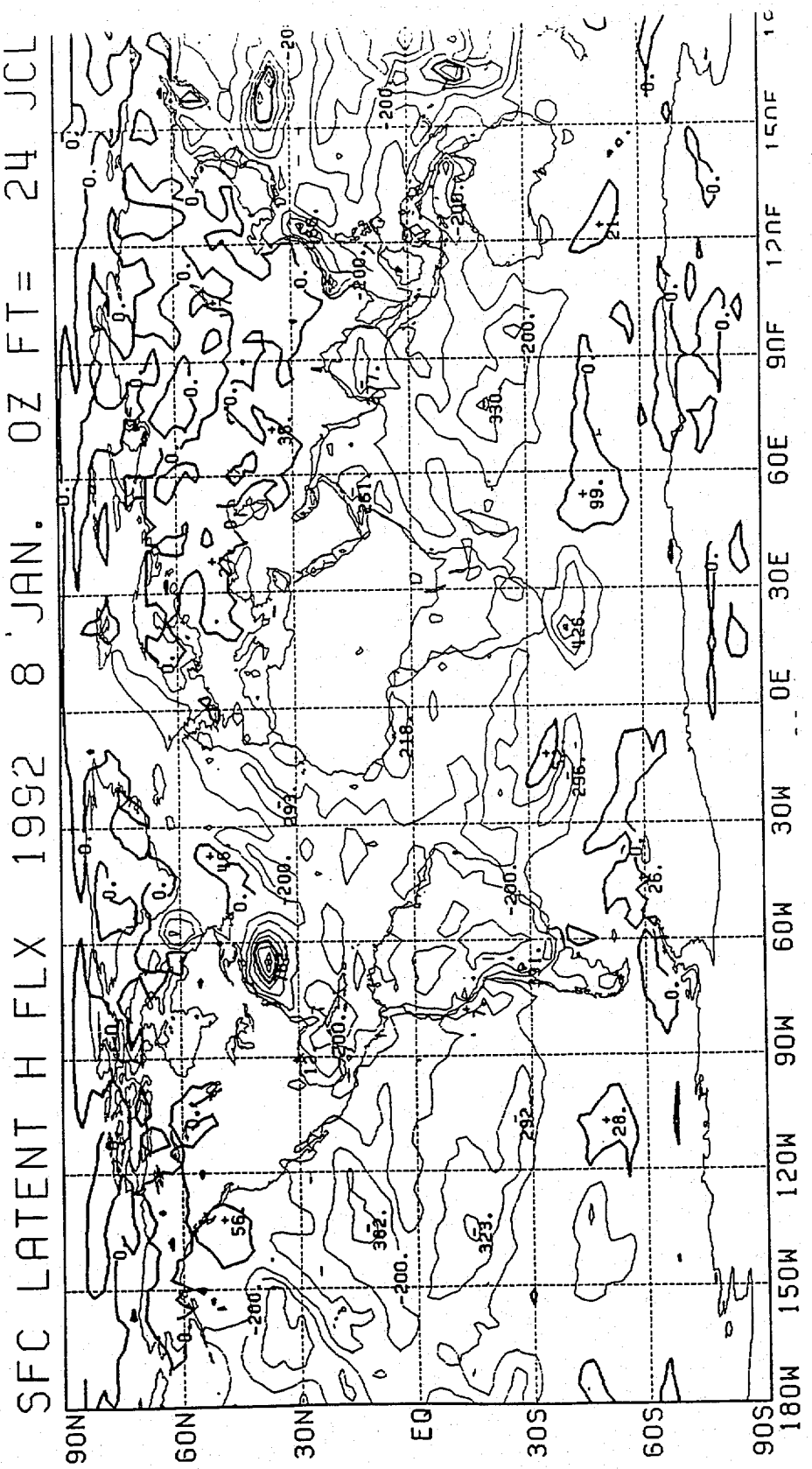
SFC LATENT H FLX 1992 8 JAN. 0Z FT= 24 JCL
90N
60N
30N
EQ
30S
60S
90S
180W
150W
120W
90W
60W
30W
0E
30E
60E
90E
120E
150E

Figure 5b.

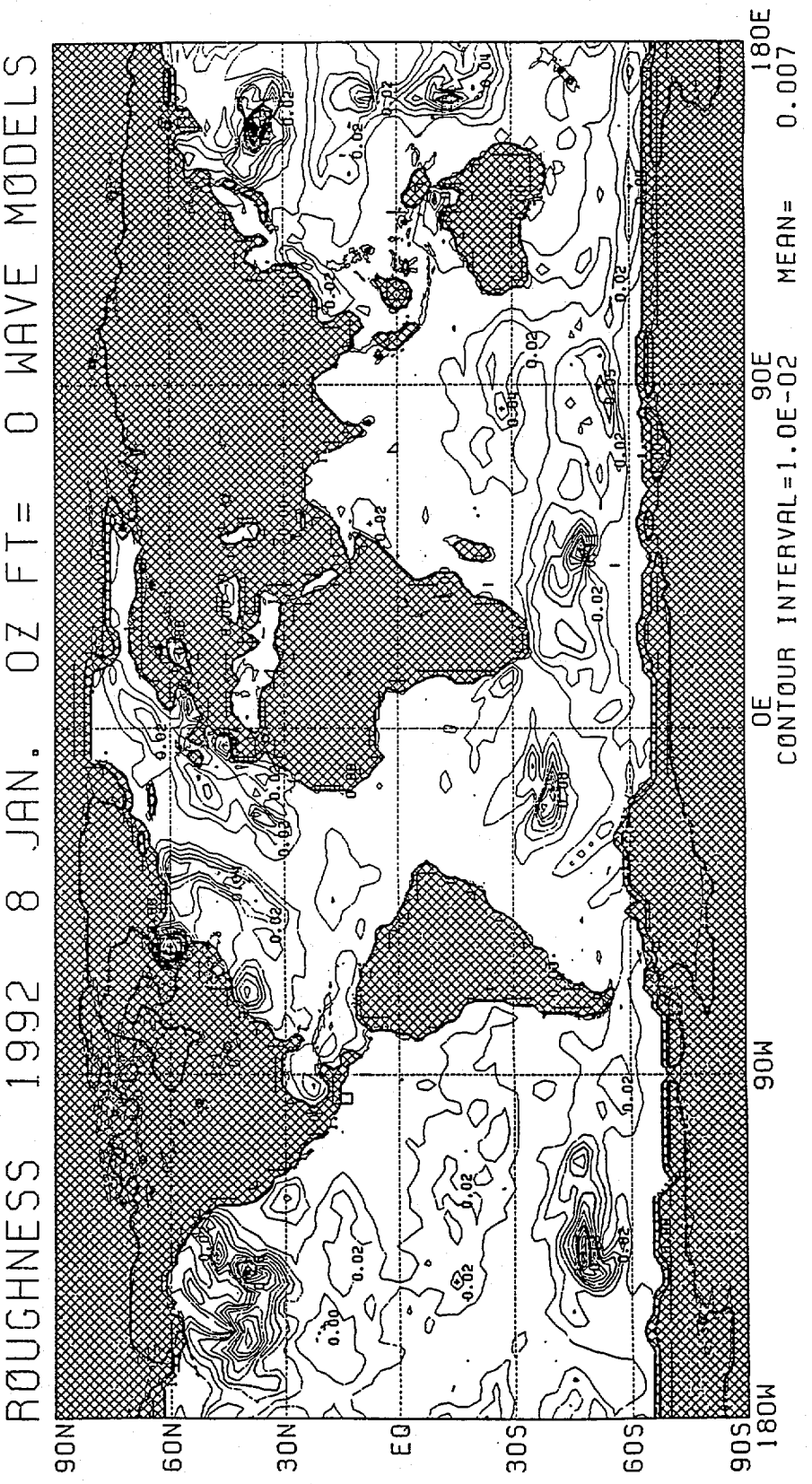
ROUGHNESS 1992 8 JAN. OZ FT= 0 WAVE MODELS
CONTOUR INTERVAL=1.0E-02 MEAN= 0.007
90N
60N
30N
EQ
30S
60S
90S
180W
90W
0E
90E
180E

Figure 6a.

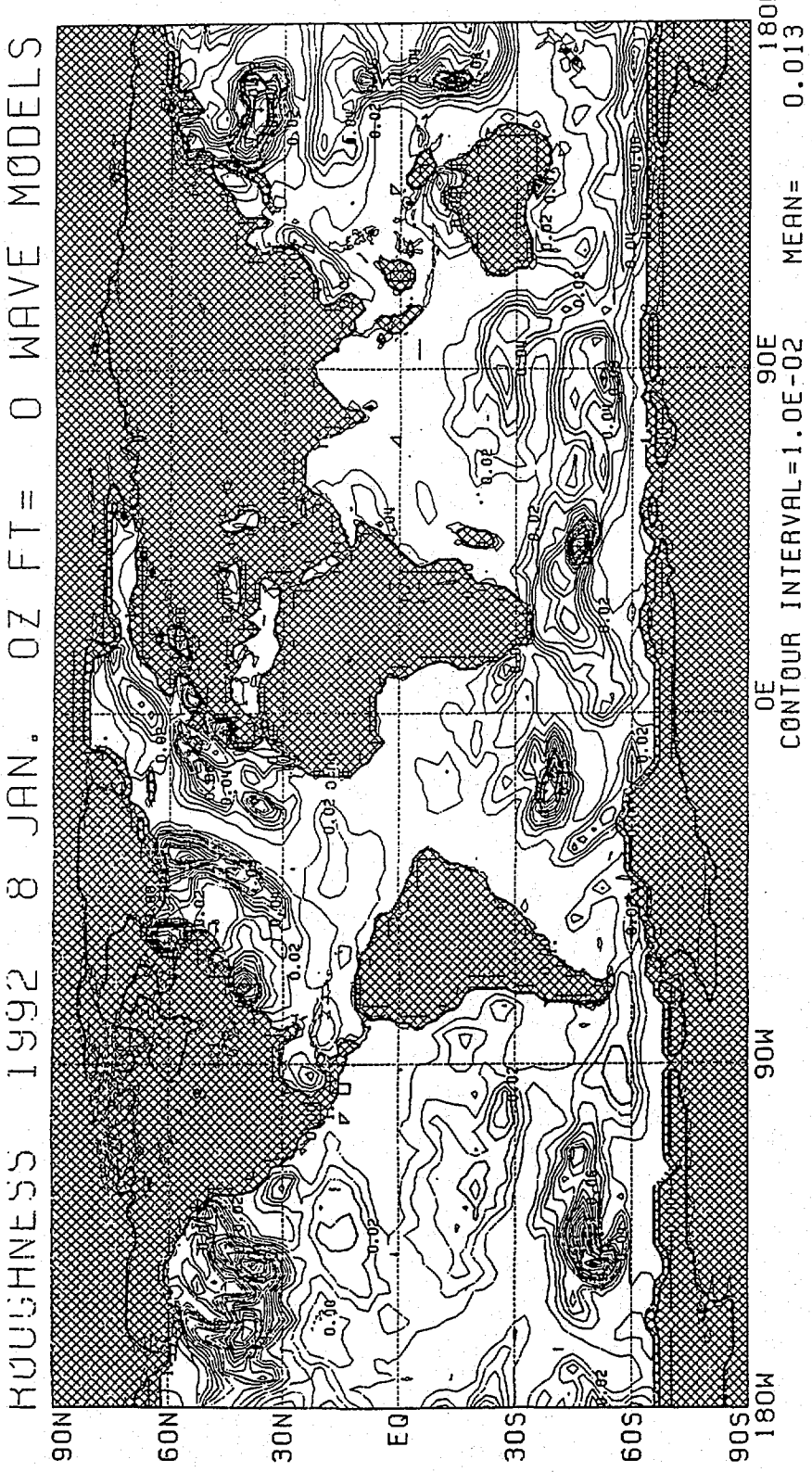
ROUGHNESS 1992 8 JAN. 0Z FT= 0 WAVE MODELS
90N
60N
30N
EQ
30S
60S
90S
180W
90W
0E
90E
180
CONTOUR INTERVAL=1.0E-02
MEAN= 0.013

Figure 6b.

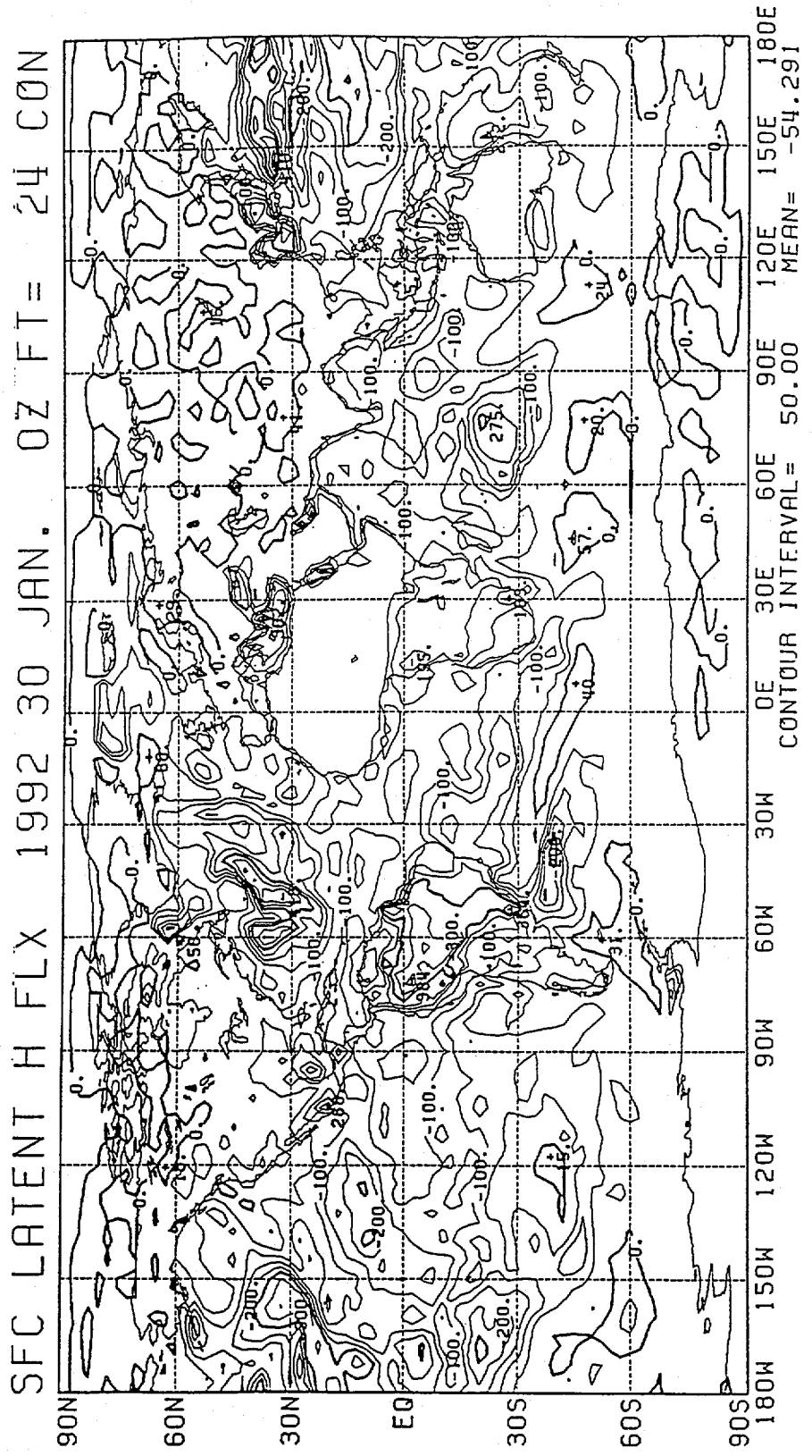
SFC LATENT H FLX 1992 30 JAN. 0Z FT= 24 CON
90N
60N
30N
EQ
30S
60S
90S
180W 150W 120W 90W 60W 30W 0E 30E 60E 90E 120E 150E 180E
CONTOUR INTERVAL= 50.00
MEAN= -54.291

Figure 7a.

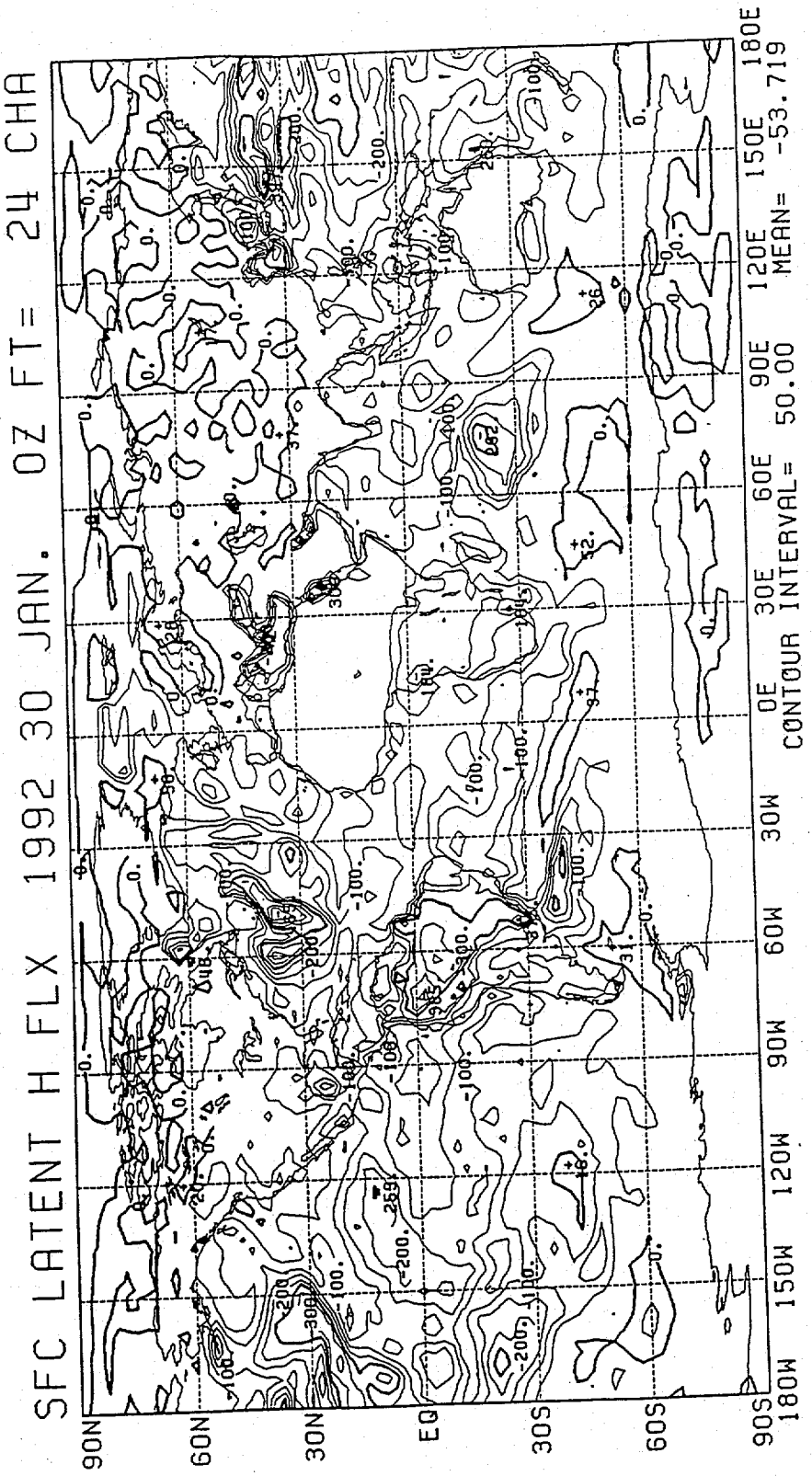
SFC LATENT H FLX 1992 30 JAN. 0Z FT= 24 CHA
90N
60N
30N
EQ
30S
60S
90S
180W 150W 120W 90W 60W 30W 0E 30E 60E 90E 120E 150E 180E
CONTOUR INTERVAL= 50.00
MEAN= -53.719

Figure 7b.

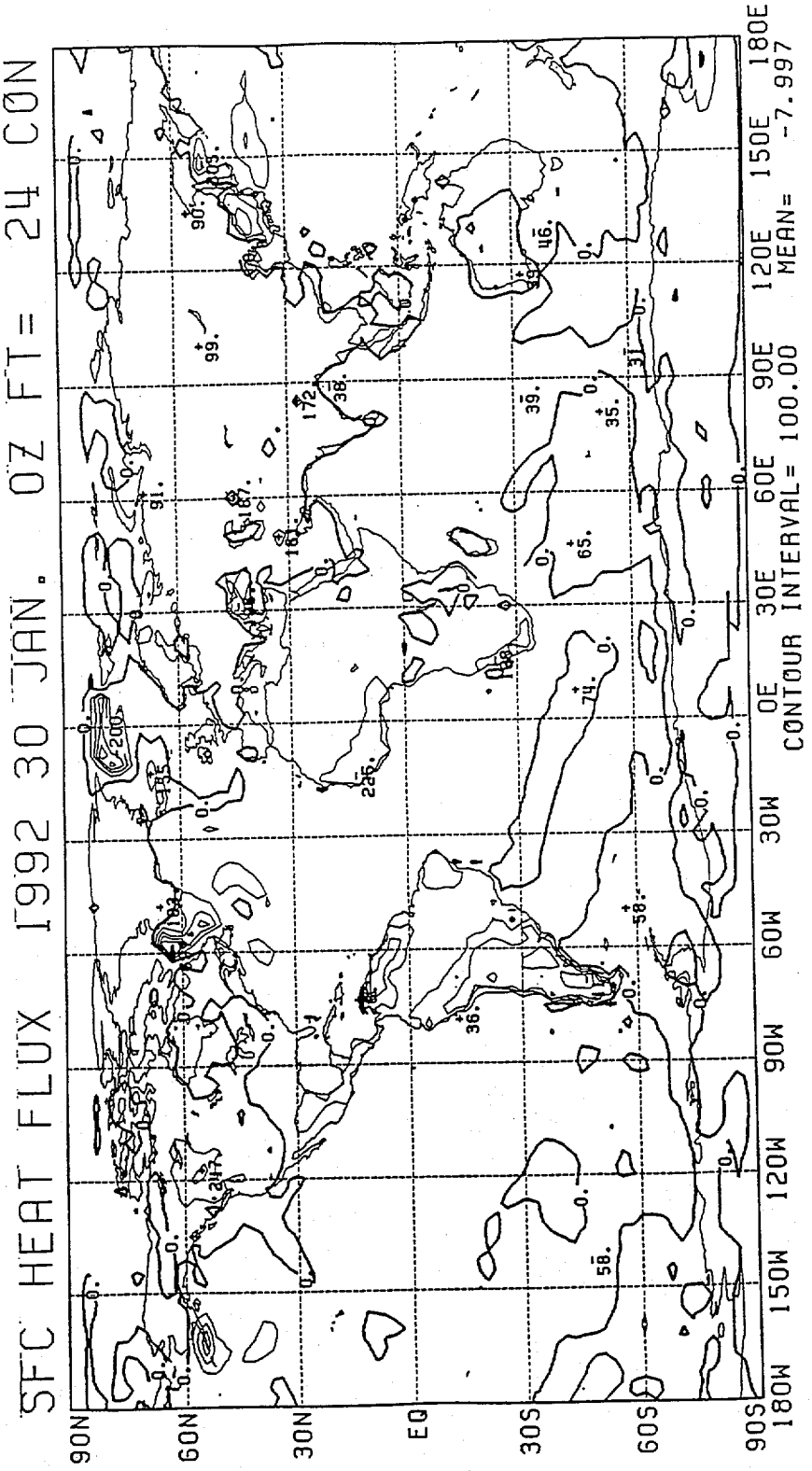
SFC HEAT FLUX 1992 30 JAN. 0Z FT= 24 CON
90N
60N
30N
EQ
30S
60S
90S
180W 150W 120W 90W 60W 30W 0E 30E 60E 90E 120E 150E 180E
CONTOUR INTERVAL= 100.00
MEAN= -7.997

Figure 8a.

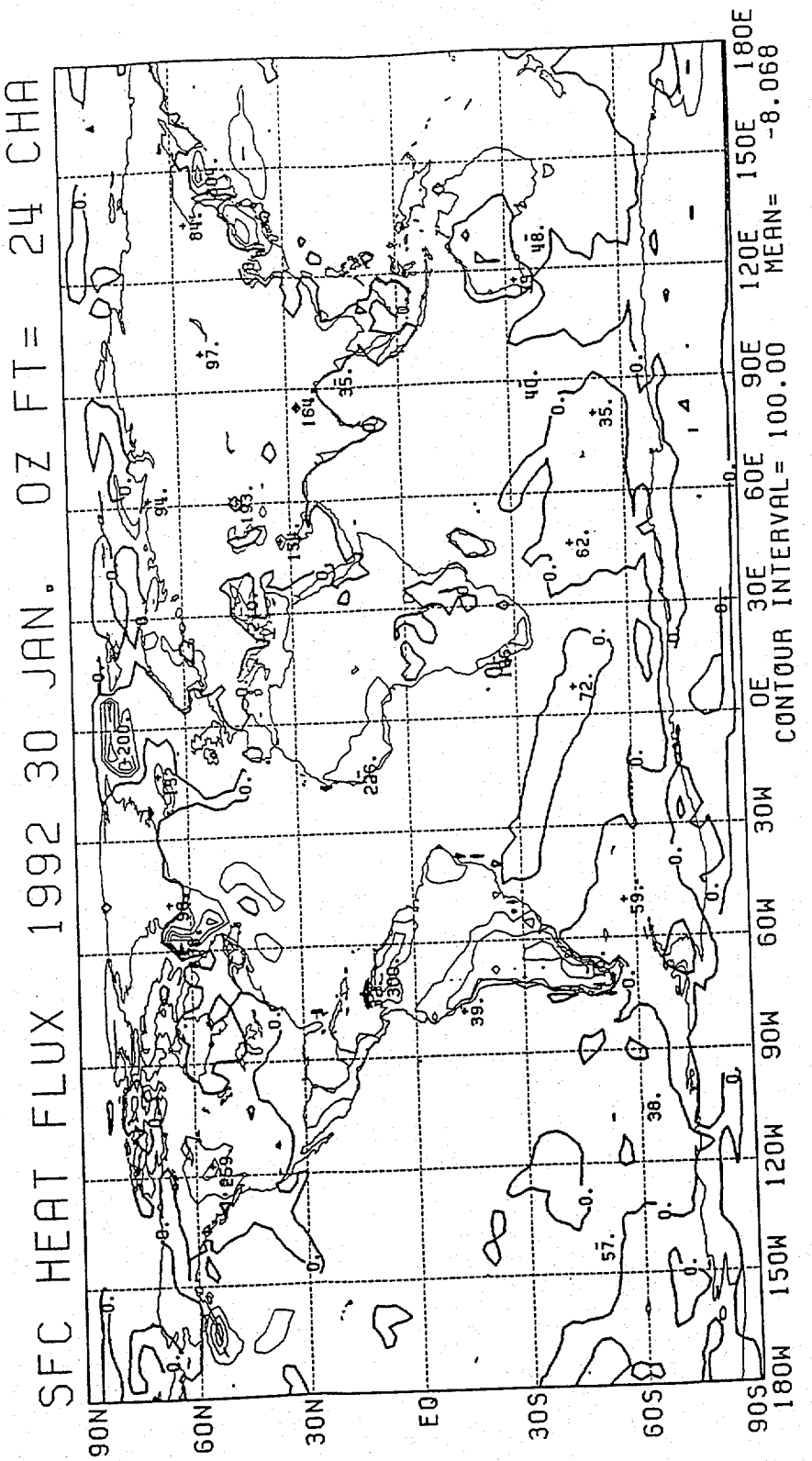
SFC HEAT FLUX 1992 30 JAN. 0Z FT= 24 CHA
90N
60N
30N
EQ
30S
60S
90S
180W
150W
120W
90W
60W
30W
0E
30E
60E
90E
120E
150E
180E
CONTOUR INTERVAL= 100.00
MEAN= -8.068

Figure 8b.

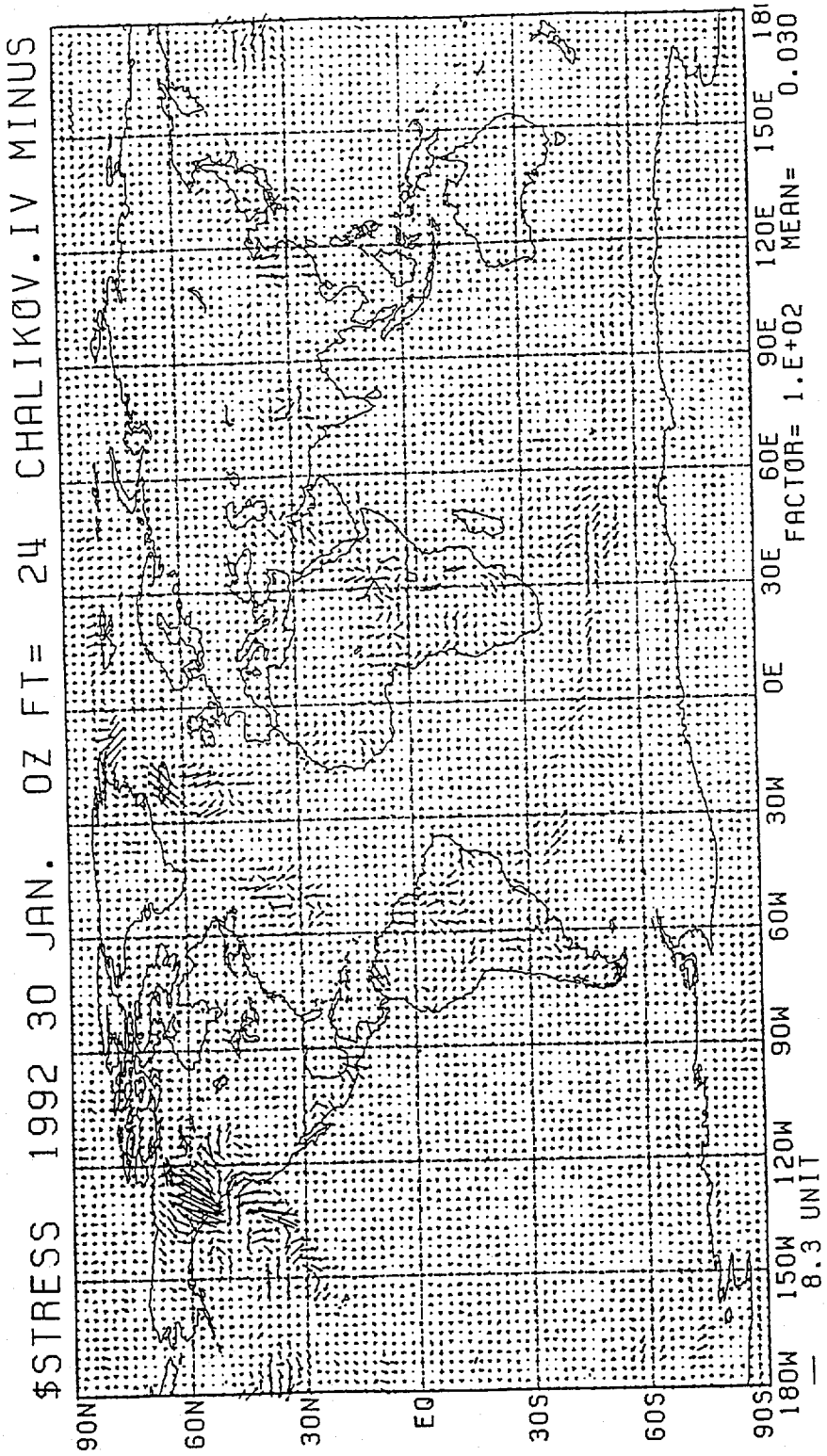
$STRESS 1992 30 JAN. OZ FT= 24 CHALIKOV.IV MINUS
90N
60N
30N
E0
30S
60S
90S
180W 150W 120W 90W 60W 30W 0E 30E 60E 90E 120E 150E 18
8.3 UNIT
FACTOR= 1.E+02 MEAN= 0.030

Figure 9.

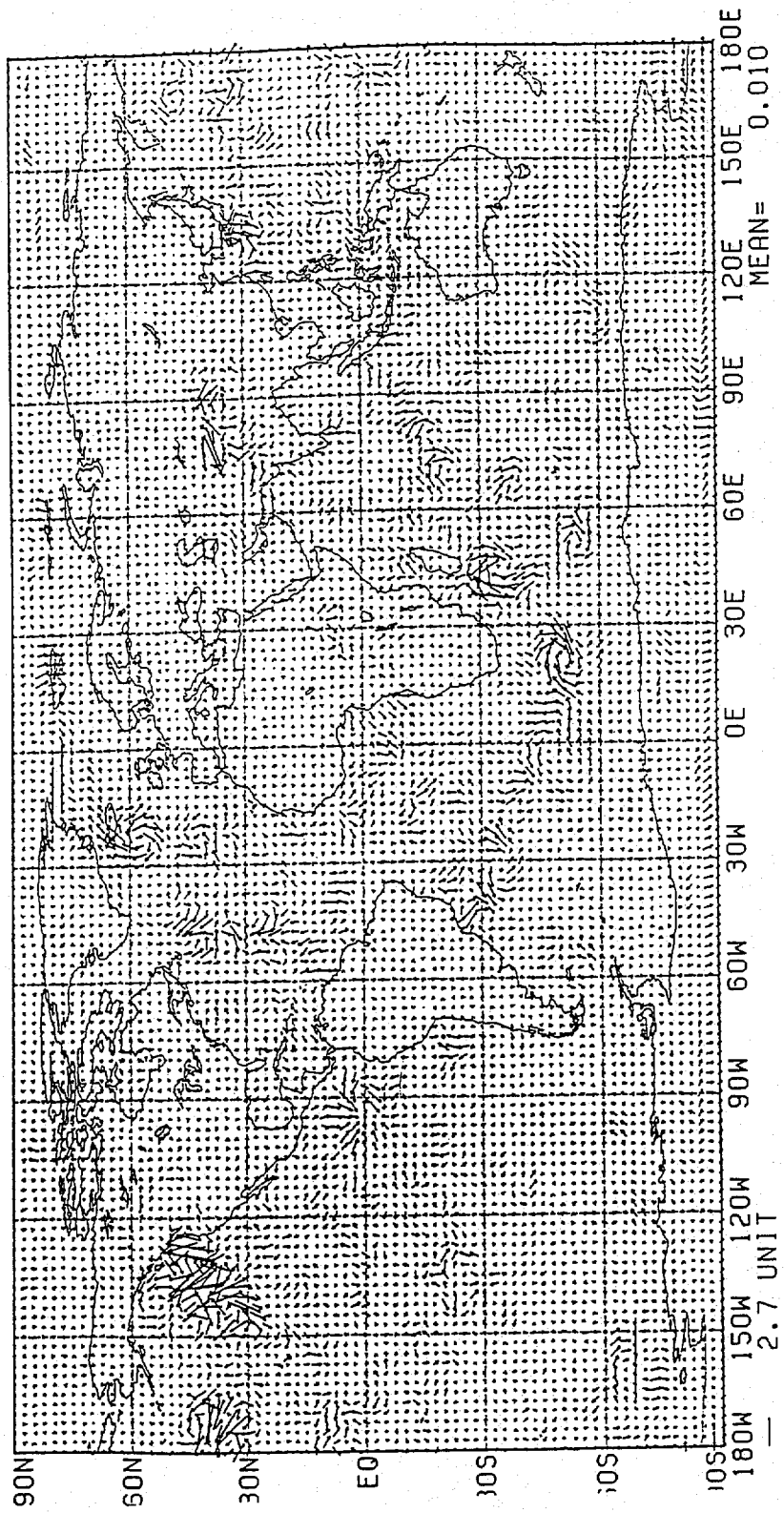
$10 METER WIND 1992 30 JAN. OZ FT= 0 CHALIKOV.IV MINUS
90N
60N
30N
EQ
30S
60S
90S
180W 150W 120W 90W 60W 30W 0E 30E 60E 90E 120E 150E 180E
2.7 UNIT
MEAN= 0.010

Figure 10.

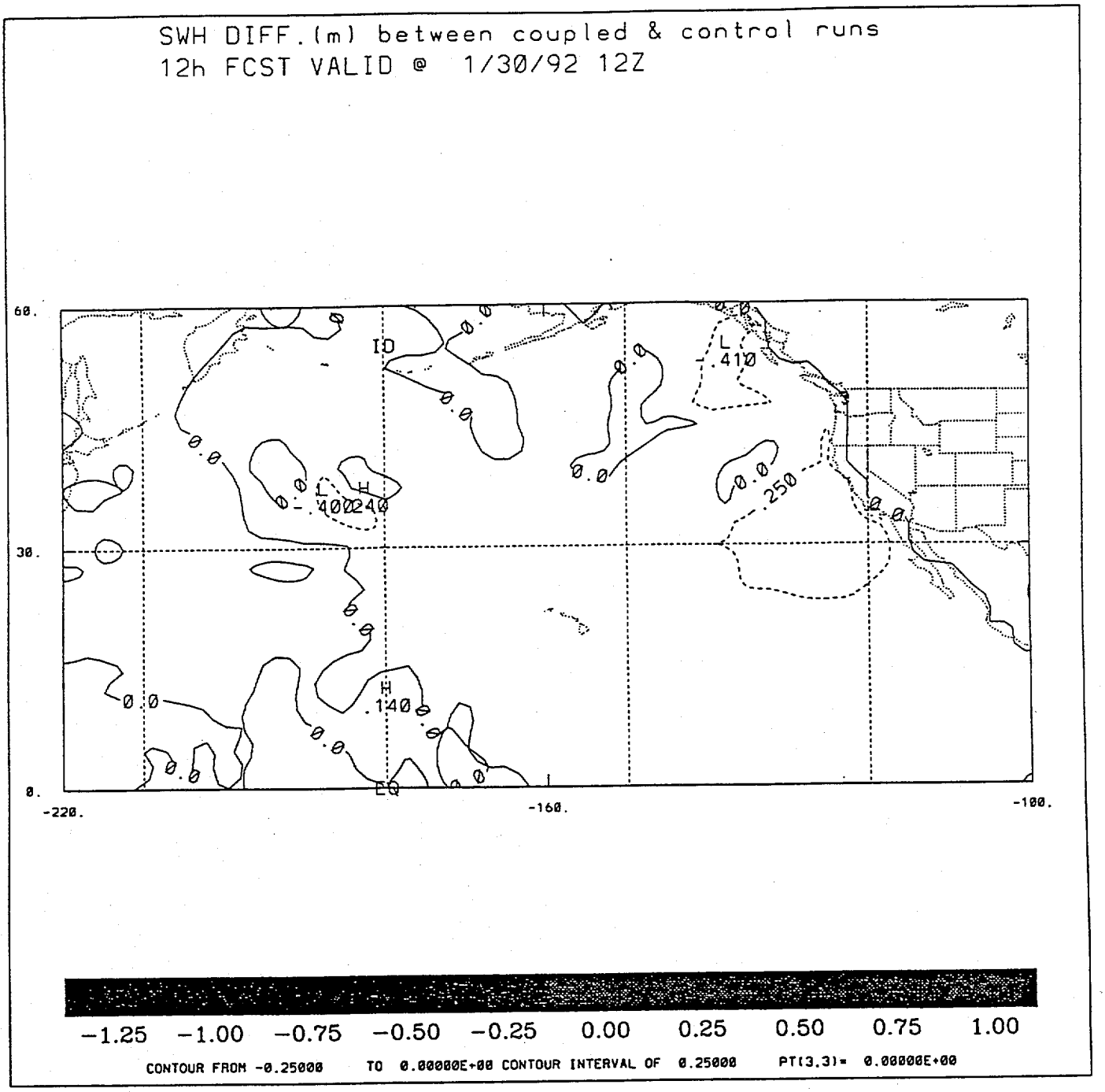
SWH DIFF.(m) between coupled & control runs
12h FCST VALID @ 1/30/92 12Z
60.
30.
0.
-220.
-160.
-100.
ID
L
.410
H
.400
.240
.250
H
.140
EQ
-1.25 -1.00 -0.75 -0.50 -0.25 0.00 0.25 0.50 0.75 1.00
CONTOUR FROM -0.25000 TO 0.00000E+00 CONTOUR INTERVAL OF 0.25000 PT(3,3)= 0.00000E+00

Figure 11a.

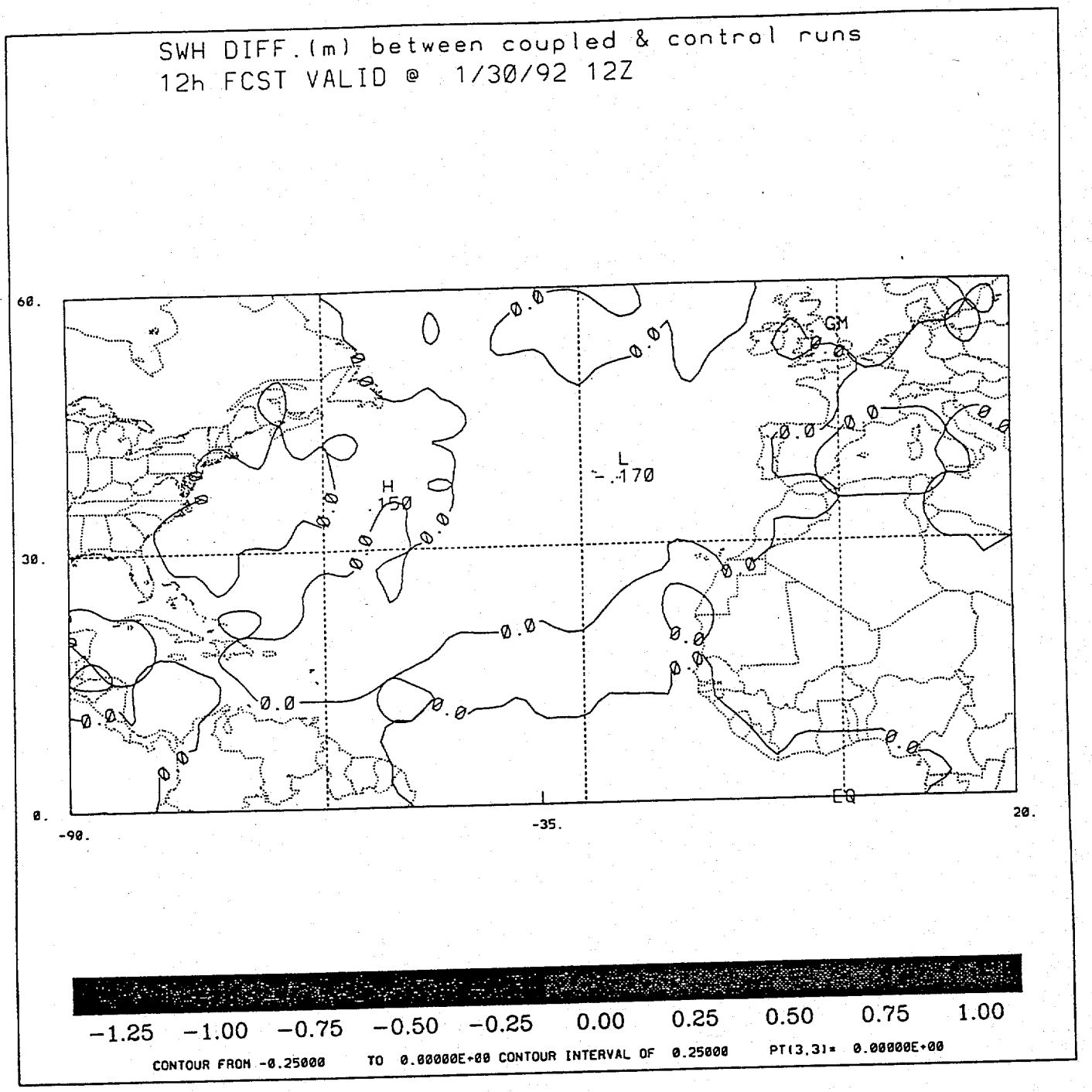
SWH DIFF.(m) between coupled & control runs
12h FCST VALID @ 1/30/92 12Z
60.
30.
0.
-90.
-35.
20.
EQ
GM
H
150
L
170
-1.25
-1.00
-0.75
-0.50
-0.25
0.00
0.25
0.50
0.75
1.00
CONTOUR FROM -0.25000 TO 0.00000E+00 CONTOUR INTERVAL OF 0.25000 PT(3,3)= 0.00000E+00

Figure 11b.

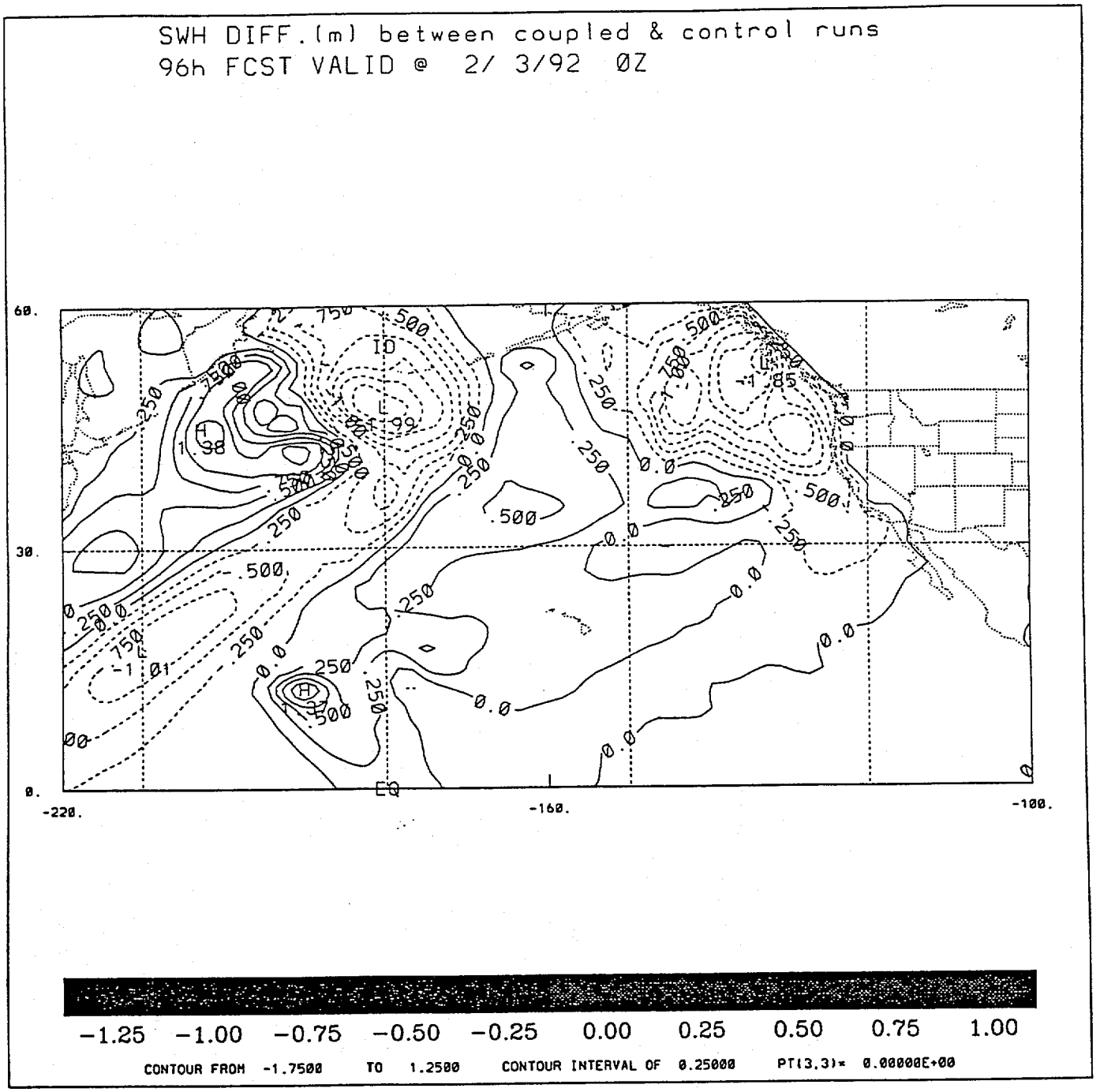
SWH DIFF.(m) between coupled & control runs
96h FCST VALID @ 2/ 3/92 0Z
60.
30.
0.
-220.
-160.
-100.
EQ
-1.25 -1.00 -0.75 -0.50 -0.25 0.00 0.25 0.50 0.75 1.00
CONTOUR FROM -1.7500 TO 1.2500 CONTOUR INTERVAL OF 0.25000 PT(3,3)= 0.00000E+00

Figure 12a.

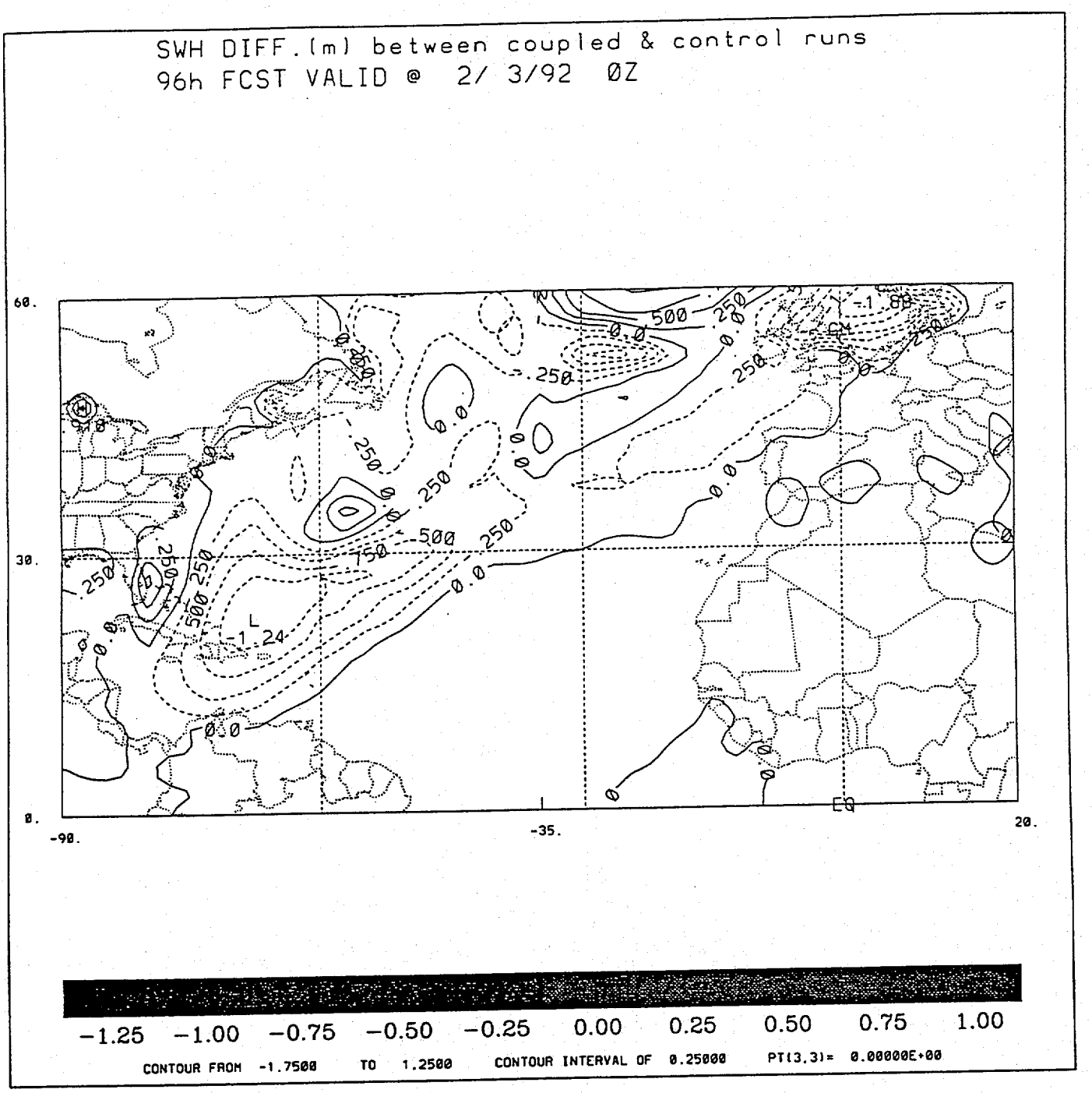
SWH DIFF.(m) between coupled & control runs
96h FCST VALID @ 2/ 3/92 0Z
60.
30.
0.
-90.
-35.
20.
-1.88
-1.24
L
H
EQ
-1.25 -1.00 -0.75 -0.50 -0.25 0.00 0.25 0.50 0.75 1.00
CONTOUR FROM -1.7500 TO 1.2500 CONTOUR INTERVAL OF 0.25000 PT(3,3)= 0.00000E+00

Figure 12b.

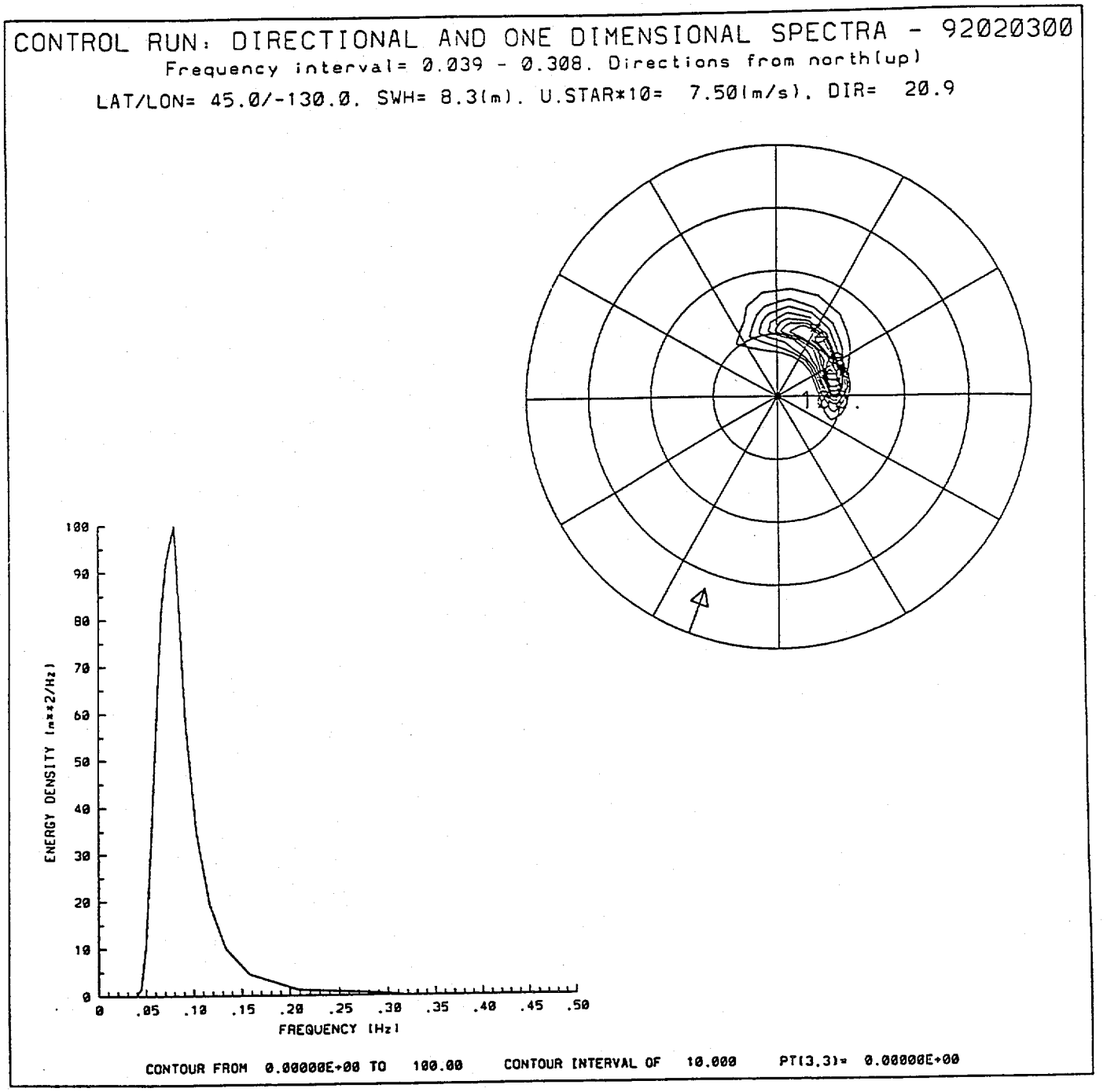
CONTROL RUN: DIRECTIONAL AND ONE DIMENSIONAL SPECTRA - 92020300
Frequency interval= 0.039 - 0.308. Directions from north(up)
LAT/LON= 45.0/-130.0. SWH= 8.3(m). U.STAR*10= 7.50(m/s). DIR= 20.9
ENERGY DENSITY (m**2/Hz)
FREQUENCY (Hz)
CONTOUR FROM 0.00000E+00 TO 100.00 CONTOUR INTERVAL OF 10.000 PT(3,3)= 0.00000E+00

Figure 13a.

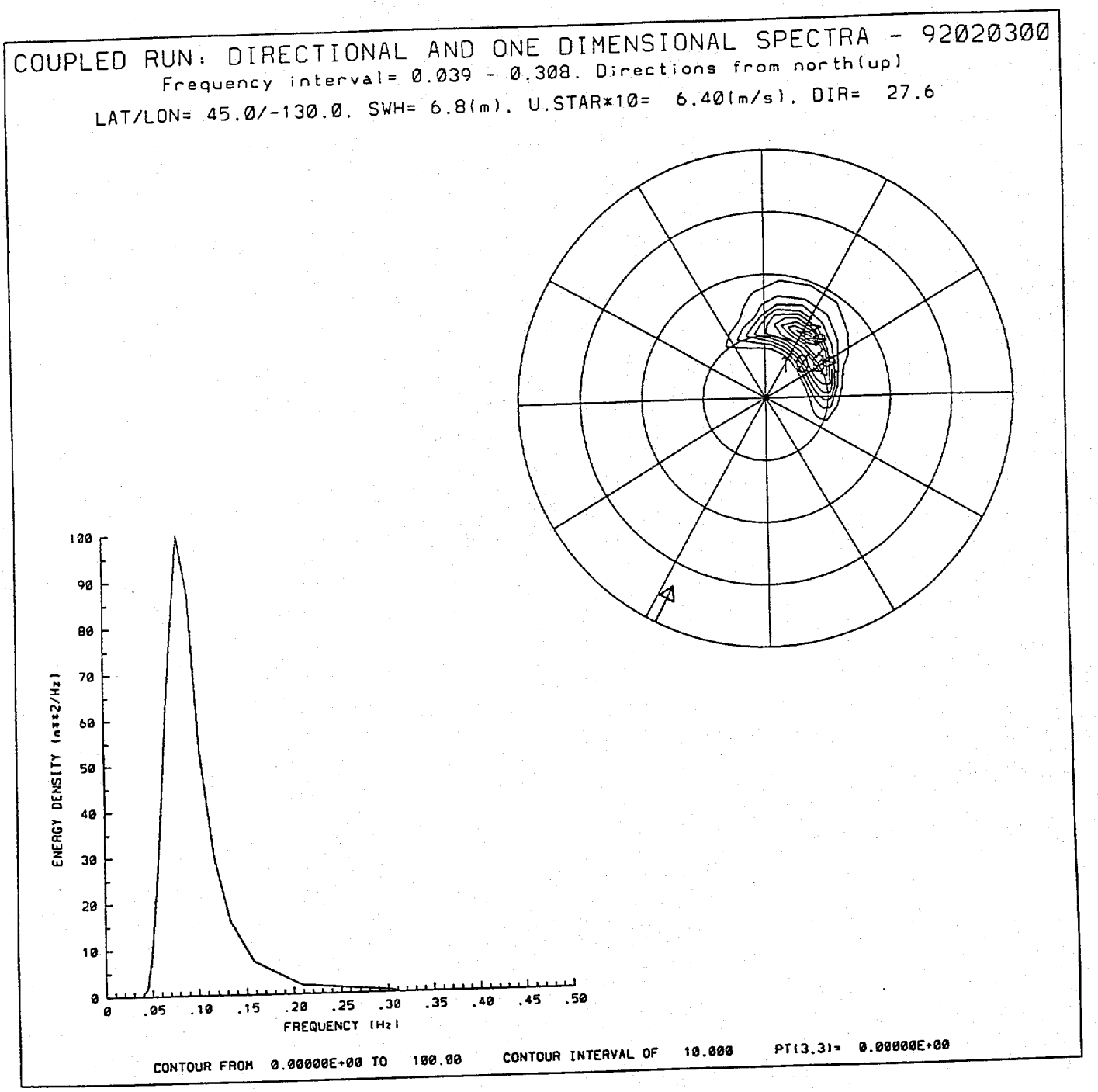
COUPLED RUN: DIRECTIONAL AND ONE DIMENSIONAL SPECTRA - 92020300
Frequency interval= 0.039 - 0.308. Directions from north(up)
LAT/LON= 45.0/-130.0. SWH= 6.8(m). U.STAR*10= 6.40(m/s). DIR= 27.6
ENERGY DENSITY (m**2/Hz)
100
90
80
70
60
50
40
30
20
10
0
0 .05 .10 .15 .20 .25 .30 .35 .40 .45 .50
FREQUENCY (Hz)
CONTOUR FROM 0.00000E+00 TO 100.00 CONTOUR INTERVAL OF 10.000 PT(3,3)= 0.00000E+00

Figure 13b.

OPC Contributions (Cont.)

No. 19. Esteva, D.C., 1988: Evaluation of Priliminary Experiments Assimilating Seasat Significant Wave Height into a Spectral Wave Model. Journal of Geophysical Research, 93, 14,099-14,105

No. 20. Chao, Y.Y., 1988: Evaluation of Wave Forecast for the Gulf of Mexico. Proceedings Fourth Conference Meteorology and Oceanography of the Coastal Zone, 42-49

No. 21. Breaker, L.C., 1989: El Nino and Related Variability in Sea-Surface Temperature Along the Central California Coast. PACLIM Monograph of Climate Variability of the Eastern North Pacific and Western North America, Geophysical Monograph 55, AGU, 133-140.

No. 22. Yu, T.W., D.C. Esteva, and R.L. Teboulle, 1991: A Feasibility Study on Operational Use of Geosat Wind and Wave Data at the National Meteorological Center. Technical Note/NMC Office Note No. 380, 28pp.

No. 23. Burroughs, L. D., 1989: Open Ocean Fog and Visibility Forecasting Guidance System. Technical Note/NMC Office Note No. 348, 18pp.

No. 24. Gerald, V. M., 1987: Synoptic Surface Marine Data Monitoring. Technical Note/NMC Office Note No. 335, 10pp.

No. 25. Breaker, L. C., 1989: Estimating and Removing Sensor Induced Correlation form AVHRR Data. Journal of Geophysical Reseach, 95, 9701-9711.

No. 26. Chen, H. S., 1990: Infinite Elements for Water Wave Radiation and Scattering. International Journal for Numerical Methods in Fluids, 11, 555-569.

No. 27. Gemmill, W.H., T.W. Yu, and D.M. Feit, 1988: A Statistical Comparison of Methods for Determining Ocean Surface Winds. Journal of Weather and Forecasting, 3, 153-160.

No. 28. Rao. D. B., 1989: A Review of the Program of the Ocean Products Center. Weather and Forecasting, 4, 427-443.

No. 29. Chen, H. S., 1989: Infinite Elements for Combined Diffration and Refraction . Conference Preprint, Seventh International Conference on Finite Element Methods Flow Problems, Huntsville, Alabama, 6pp.

NO. 30. Chao, Y. Y., 1989: An Operational Spectral Wave Forecasting Model for the Gulf of Mexico. Proceedings of 2nd International Workshop on Wave Forecasting and Hindcasting, 240-247.

No. 31. Esteva, D. C., 1989: Improving Global Wave Forecasting Incorporating Altimeter Data. Proceedings of 2nd International Workshop on Wave Hindcasting and Forecasting, Vancouver, B.C., April 25-28, 1989, 378-384.

No. 32. Richardson, W. S., J. M. Nault, D. M. Feit, 1989: Computer-Worded Marine Forecasts. Preprint, 6th Symp. on Coastal Ocean Management Coastal Zone 89, 4075-4084.

No. 33. Chao, Y. Y., T. L. Bertucci, 1989: A Columbia River Entrance Wave Forecasting Program Developed at the Ocean Products Center. Techical Note/NMC Office Note 361.

No. 34. Burroughs, L. D., 1989: Forecasting Open Ocean Fog and Visibility. Preprint, 11th Conference on Probability and Statisitcs, Monterey, Ca., 5pp.

No. 35. Rao, D. B., 1990: Local and Regional Scale Wave Models. Proceeding (CMM/WMO) Technical Conference on Waves, WMO, Marine Meteorological of Related Oceanographic Activities Report No. 12, 125-138.

OPC CONTRIBUTIONS (Cont.)

No. 36. Burroughs, L.D., 1991: Forecast Guidance for Santa Ana conditions. Technical Procedures Bulletin No. 391, 11pp.

No. 37. Burroughs, L. D., 1989: Ocean Products Center Products Review Summary. Technical Note/NMC Office Note No. 359. 29pp.

No. 38. Feit, D. M., 1989: Compendium of Marine Meteorological and Oceanographic Products of the Ocean Products Center (revision 1). NOAA Technical Memo NWS/NMC 68.

No. 39. Esteva, D. C., Y. Y. Chao, 1991: The NOAA Ocean Wave Model Hindcast for LEWEX. Directional Ocean Wave Spectra, Johns Hopkins University Press, 163-166.

No. 40. Sanchez, B. V., D. B. Rao, S. D. Steenrod, 1987: Tidal Estimation in the Atlantic and Indian Oceans, 3° x 3° Solution. NASA Technical Memorandum 87812, 18pp.

No. 41. Crosby, D.S., L.C. Breaker, and W.H. Gemmill, 1990: A Difintion for Vector Correlation and its Application to Marine Surface Winds. Technical Note/NMC Office Note No. 365, 52pp.

No. 42. Feit, D.M., and W.S. Richardson, 1990: Expert System for Quality Control and Marine Forecasting Guidance. Preprint, 3rd Workshop Operational and Metoerological, CMOS, 6pp.

No. 43. Gerald, V.M., 1990: OPC Unified Marine Database Verification System. Technical Note/NMC Office Note No. 368, 14pp.

No. 44. Wohl, G.M., 1990: Sea Ice Edge Forecast Verification System. National Weather Association Digest, (submitted)

No. 45. Feit, D.M., and J.A. Alpert, 1990: An Operational Marine Fog Prediction Model. NMC Office Note No. 371, 18pp.

No. 46. Yu, T. W. , and R. L. Teboulle, 1991: Recent Assimilation and Forecast Experiments at the National Meteorological Center Using SEASAT-A Scatterometer Winds. Technical Note/NMC Office Note No. 383, 45pp.

No. 47. Chao, Y.Y., 1990: On the Specification of Wind Speed Near the Sea Surface. Marine Forecaster Training Manual, (submitted)

No. 48. Breaker, L.C., L.D. Burroughs, T.B. Stanley, and W.B. Campbell, 1992: Estimating Surface Currents in the Slope Water Region Between 37 and 41°N Using Satellite Feature Tracking. Technical Note, 47pp.

No. 49. Chao, Y.Y., 1990: The Gulf of Mexico Spectral Wave Forecast Model and Products. Technical Procedures Bulletin No. 381, 3pp.

No. 50. Chen, H.S., 1990: Wave Calculation Using WAM Model and NMC Wind. Preprint, 8th ASCE Engineering Mechanical Conference, 1, 368-372.

No. 51. Chao, Y.Y., 1990: On the Transformation of Wave Spectra by Current and Bathymetry. Preprint, 8th ASCE Engineering Mechnical Conference, 1, 333-337.

No. 52. Breaker, L.C., W.H. Gemmill, and D.S. Crosby, 1990: A Vector Correlation Coefficient in Geophysical: Theoretical Background and Application. Deep Sea Research, (to be submitted)

No. 53. Rao, D.B., 1991: Dynamical and Statistical Prediction of Marine Guidance Products. Proceedings, IEEE Conference Oceans 91, 3, 1177-1180.

No. 54. Gemmill, W.H., 1991: High-Resolution Regional Ocean Surface Wind Fields. Proceedings, AMS 9th Conference on Numerical Weather Prediction, Denver, CO, Oct. 14-18, 1991, 190-191.

No. 55. Yu, T.W., and D. Deaven, 1991: Use of SSM/I Wind Speed Data in NMC's GDAS. Proceedings, AMS 9th Conference on Numerical Weather Prediction, Denver, CO, Oct. 14-18, 1991, 416-417.

No. 56. Burroughs, L.D., and J.A. Alpert, 1992: Numerical Fog and Visiability Guidance in Coastal Regions. Technical Procedures Bulletin. (to be submitted)

No. 57. Chen, H.S., 1992: Taylor-Gelerkin Method for Wind Wave Propagation. ASCE 9th Conf. Eng. Mech. (in press)

No. 58. Breaker, L.C., and W.H. Gemmill, and D.S. Crosby, 1992: A Technique for Vector Correlation and its Application to Marine Surface Winds. AMS 12th Conference on Probability and Statistics in the Atmospheric Sciences, Toronto, Ontario, Canada, June 22-26, 1992.

No. 59. Breaker, L.C., and X.-H. Yan, 1992: Surface Circulation Estimation Using Image Processing and Computer Vision Methods Applied to Sequential Satellite Imagery. Proceeding of the 1st Thematic Conference on Remote Sensing for Marine Coastal Environment, New Orleans, LA, June 15-17, 1992.

No. 60. Wohl, G., 1992: Operational Demonstration of ERS-1 SAR Imagery at the Joint Ice Center. Proceeding of the MTS 92 - Global Ocean Partnership, Washington, DC, Oct. 19-21, 1992.

No. 61. Waters, M.P., Caruso, W.H. Gemmill, W.S. Richardson, and W.G. Pichel, 1992: An Interactive Information and Processing System for the Real-Time Quality Control of Marine Meteorological Oceanographic Data. Pre-print 9th International Conference on Interactive Information and Processing System for Meteorology, Oceanography and Hydrology, Anaheim, CA, Jan 17-22, 1993.

No. 62. Breaker, L.C., and V. Krasnopolsky, 1992: The Problem of AVHRR Image Navigation Revisited. Intr. Journal of Remote Sensing (in press).

No. 63. Breaker, L.C., D.S. Crosby, and W.H. Gemmill, 1992: The Application of a New Definition for Vector Correlation to Problems in Oceanography and Meteorology. Journal of Atmospheric and Oceanic Technology (submitted).

No. 64. Grumbine, R., 1992: The Thermodynamic Predictability of Sea Ice. Journal of Glaciology, (in press).

No. 65. Chen, H.S., 1993: Global Wave Prediction Using the WAM Model and NMC Winds. 1993 International Conference on Hydro Science and Engineering, Washington, DC, June 7 - 11, 1993. (submitted)

No. 66. Krasnopolsky, V., and L.C. Breaker, 1993: Multi-Lag Predictions for Time Series Generated by a Complex Physical System using a Neural Network Approach. Journal of Physics A: Mathematical and General, (submitted).

No. 67. Breaker, L.C., and Alan Bratkovich, 1993: Coastal-Ocean Processes and their Influence on the Oil Spilled off San Francisco by the M/V Puerto Rican. Marine Environmental Research, (submitted)

No. 68. Breaker, L.C., L.D. Burroughs, J.F. Culp, N.L. Gunasso, R. Teboulle, and C.R. Wong, 1993: Surface and Near-Surface Marine Observations During Hurricane Andrew. Weather and Forecasting, (in press).

No. 69. Burroughs, L.C., and R. Nichols, 1993: The National Marine Verification Program, Technical Note, (in press).

No. 70. Gemmill, W.H., and R. Teboulle, 1993: The Operational Use of SSM/I Wind Speed Data over Oceans. Pre-print 13th Conference on Weather Analyses and Forecasting, (submitted).

No. 71. Yu, T.-W., J.C. Derber, and R.N. Hoffman, 1993: Use of ERS-1 Scatterometer Backscattered Measurements in Atmospheric Analyses. Pre-print 13th Conference on Weather Analyses and Forecasting, (submitted).

No. 72. Chalikov, D. and Y. Liberman, 1993: Director Modeling of Nonlinear Waves Dynamics. J. Physical, (submitted).

No. 73. Woiceshyn, P., T.W. Yu, W.H. Gemmill, 1993: Use of ERS-1 Scatterometer Data to Derive Ocean Surface Winds at NMC. Pre-print 13th Conference on Weather Analyses and Forecasting, (submitted).

No. 74. Grumbine, R.W., 1993: Sea Ice Prediction Physics. Technical Note, (in press)

No. 75. Chalikov, D., 1993: The Parameterization of the Wave Boundary Layer. Journal of Physical Oceanography, (to be submitted).

No. 76. Tolman, H., 1993: Modeling Bottom Friction in Wind-Wave Models. Waves 93 in New Orleans, LA, (in press).

No. 77. Breaker, L., W. Broenkow, 1993: The Circulation of Monterey Bay and Related Processes. Revised and resubmitted to Oceanography and Marine Biology: An Annual Review, (to be submitted).

No. 78. Chalikov, D., D. Esteva, M. Iredell and P. Long, 1993: Dynamic Coupling between the NMC Global Atmosphere and Spectral Wave Models. Technical Note, (to be submitted).


DEPARTMENT OF COMMERCE
UNITED STATES OF AMERICA